ANISOTROPIAS INTRÍNSECAS, DE TROCA E RODÁVEL EM INTERFACES FM/AF ANALISADAS VIA MEDIDAS E SIMULAÇÕES DE CURVAS DE HISTERESE E REMANÊNCIA MAGNÉTICA E DE FMR

J. GESHEV

Instituto de Física/UFRGS, Porto Alegre, RS, Brazil

Outline

- ✓ Magnetic Anisotropy: most important types
- ✓ Rotatable Anisotropy (RA) in bi- and trilayers films
  - ➢ magnetization and FMR data
  - ➢ negative RA
  - ➢ Training effects
- ✓ Remanence plots in exchange-coupled systems
- ✓ Temporal EB raise after light ion irradiation

Anisotropia – termo aplicado a substâncias cujas propriedades físicas variam de acordo com a direção a partir das quais são observadas (Allaby & Allaby, Dictionary of Earth Sciences, p. 622, Oxford University Press, Oxford, 1999).

A primeira aplicação de um material magnético:

Principais tipos de anisotropia magnética

1. Anisotropia **magnetocristalina**
2. Anisotropia de **forma**
3. Anisotropia de '**stress**', ou de magnetostricção
4. Anisotropia **induzida** por
   a) Tratamento térmico na presença de campo magnético aplicado ('annealing')
   b) Deformação plástica
   c) Irradiação iônica com campo magnético aplicado
5. Anisotropia de **superfície**
6. Anisotropia de **troca** (de intercâmbio, ou 'exchange anisotropy')

S. Chikazumi, *Physics of Magnetism* (Wiley, New York, 1964).
B. D. Cullity, *Introduction to Magnetic Materials* (Addison-Wesley, London, 1972).

Anisotropia de superfície

Filmes magnéticos ultra-finos ou partículas pequenas (de alguns nanômetros de tamanho) de um determinado material podem apresentar anisotropia magnética muito diferente daquela na sua forma massiva.

Em filmes finos: mudança na orientação de $\mathbf{M_s}$ para a direção normal ao plano na medida que a espessura do filme é reduzida.

- **anisotropia de superfície magnetocristalina**: resultado de redução da simetria local em superfícies e interfaces [L. Néel, J. Phys. Radium **15**, 376 (1954)];

- **anisotropia de superfície dipolar**: provém da rugosidade da superfície;

- **anisotropia de superfície magnetoelástica**: conseqüência de 'lattice mismatch'.

Exchange Bias: intuitive view

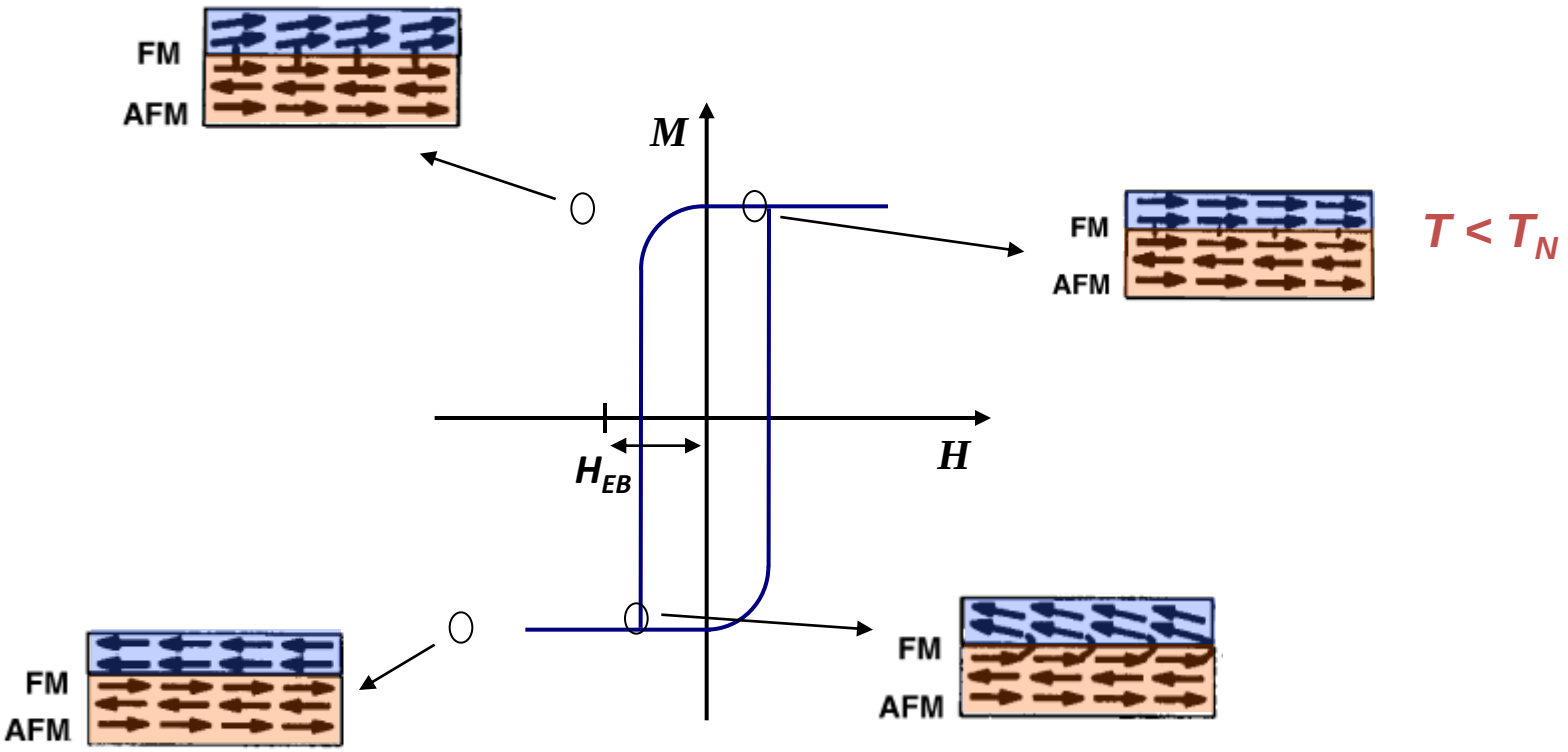

Some other EB manifestations related to this talk:

- Training and thermal effects
- Increase of the coercivity
- Isotropy shift of the FMR field
- Asymmetric hysteresis loops

EB and **RA** in **polycrystalline** AF/FM films with uncompensated spins (UCS) at the interface

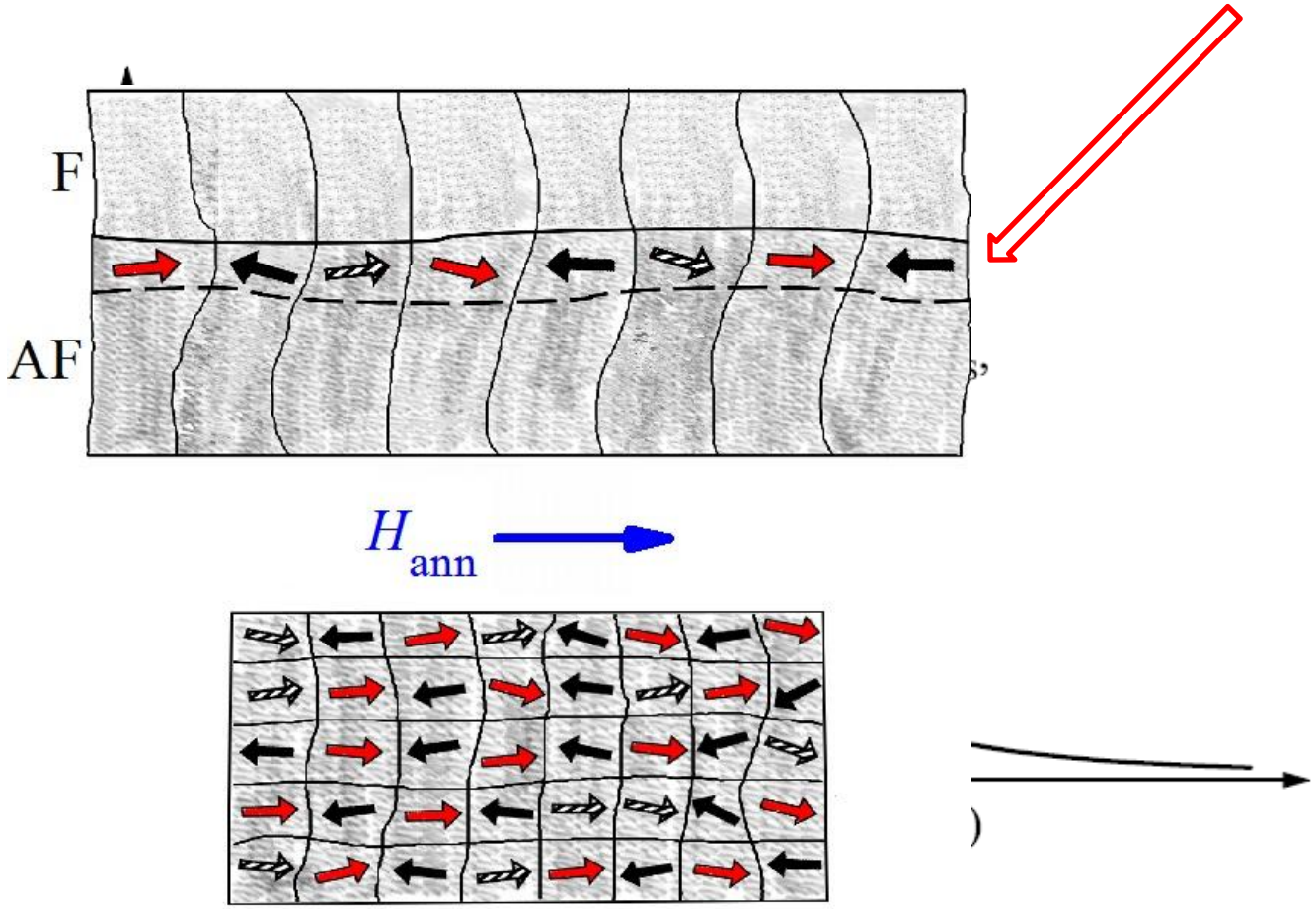

Schematic of an energy barrier distribution to the reversal of the UCS within the AF/FM interface.

J. Phys.: Condens. Matter **24** (2012) 326004 (7pp)

A polycrystalline model for magnetic exchange bias

A Harres and J Geshev

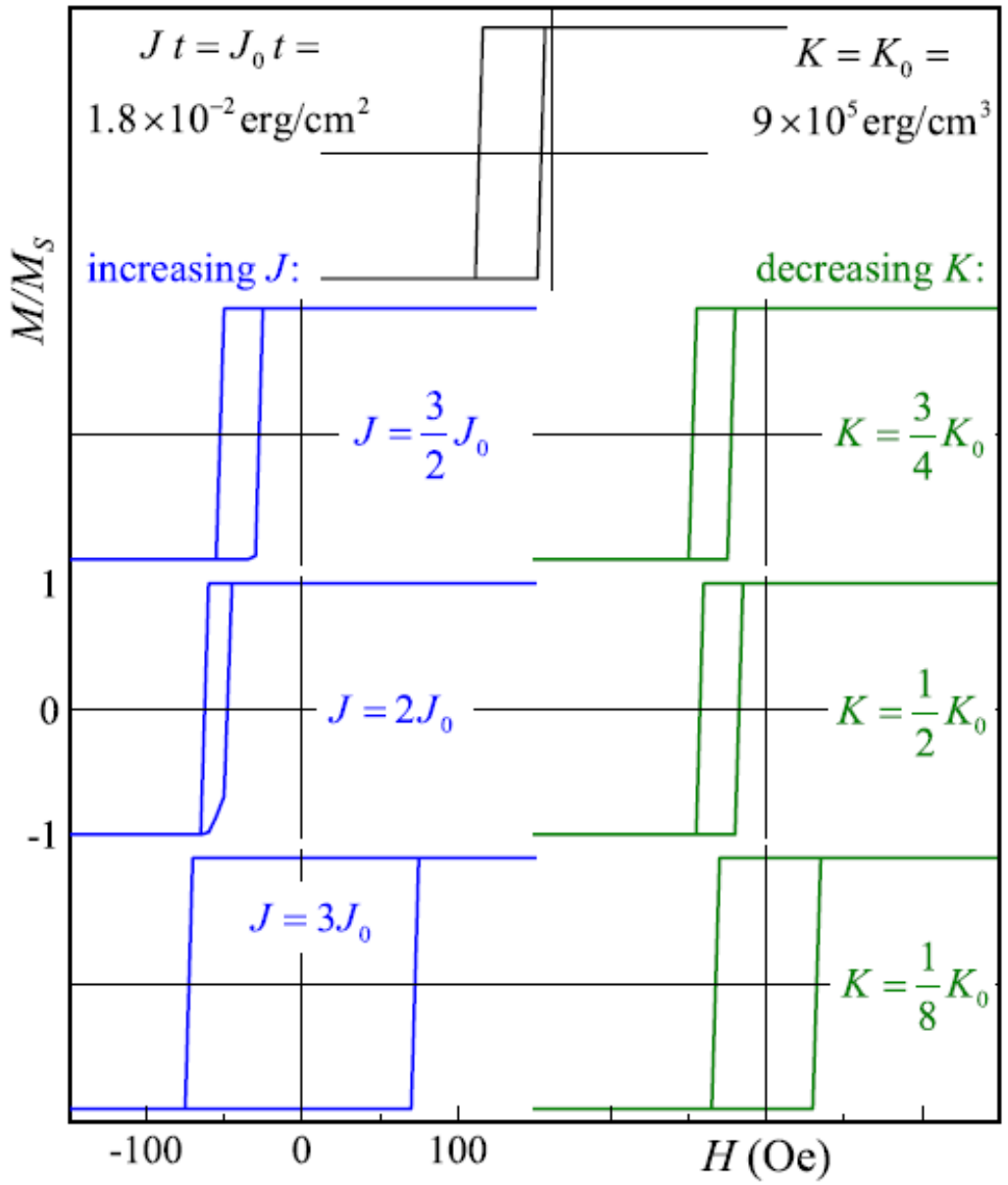

Thermal **training effect**

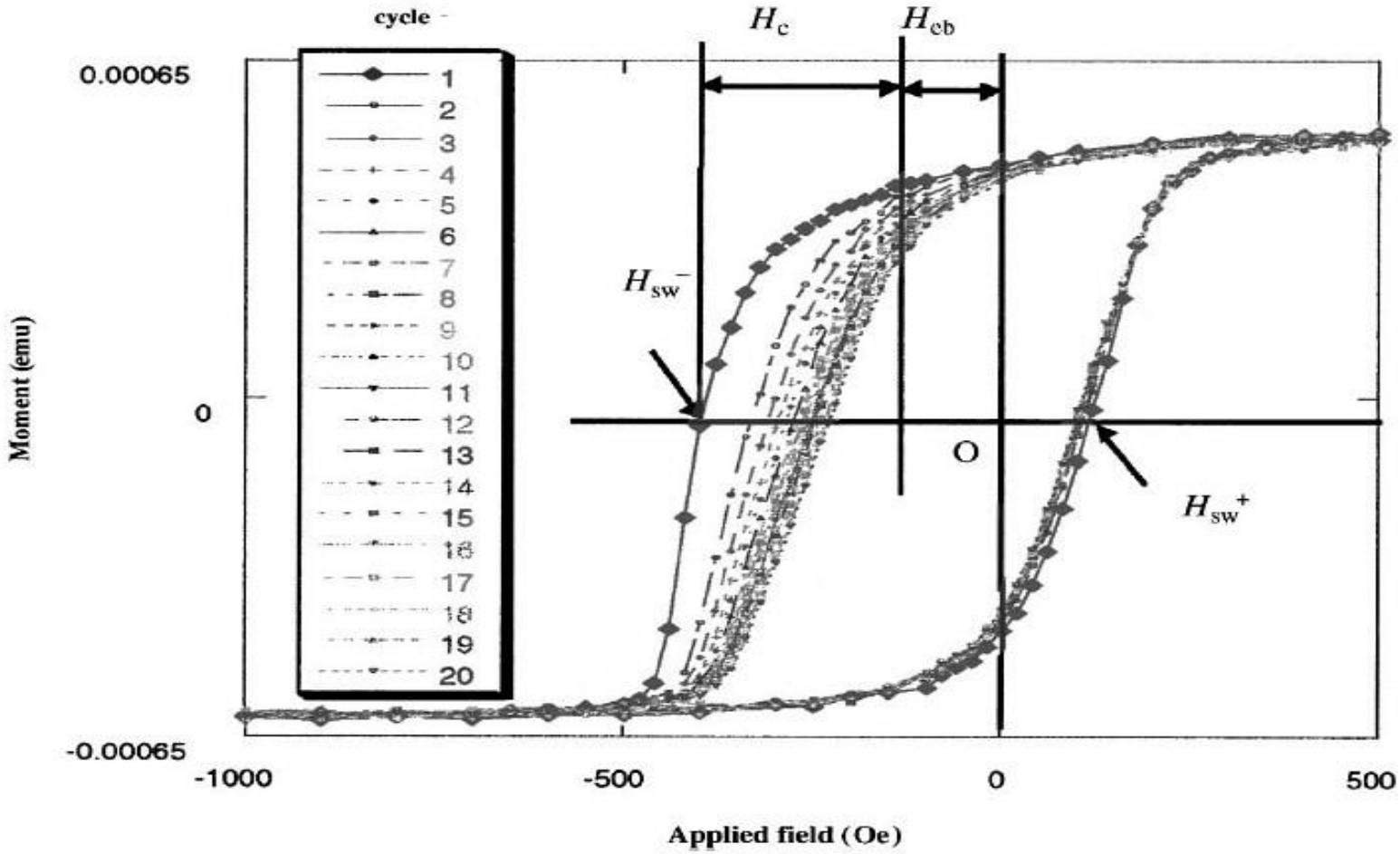

Fig. 7. A typical training effect. The definitions of H_{sw}^-, H_{sw}^+, H_{eb} (H_p) and H_c are given.

Fujiwara *et al*., Journ. Magn. Magn. Mater. **235** (2001) 319.

Thermal vs. Athermal training

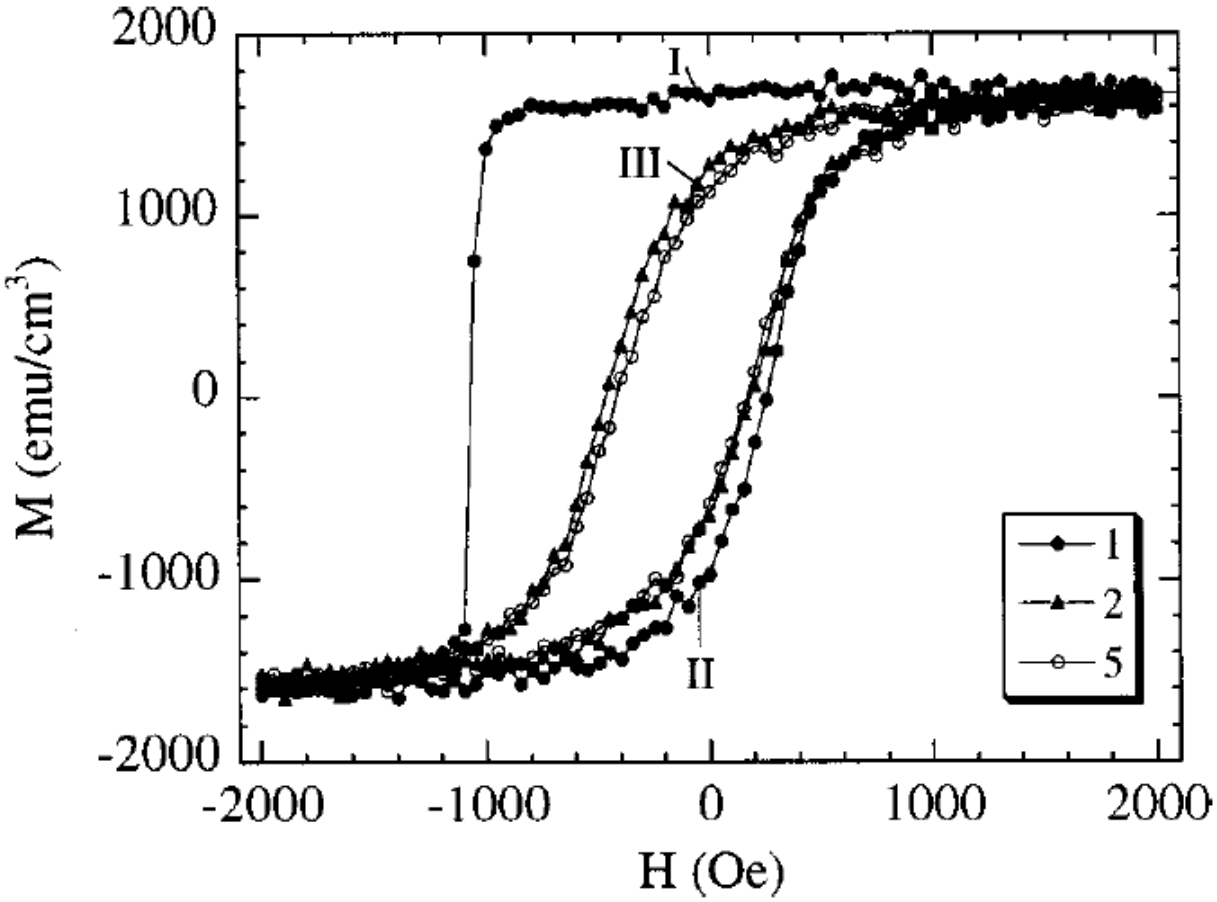

$$H_{EB}(n) = H_{EB}^{equi} + \frac{\kappa}{\sqrt{n}}$$

S. G. E. te Velthuis *et al*., Journ. Appl. Phys. **87** (2000) 5046.

CoCoO bilayer, 10 K: thermal training?

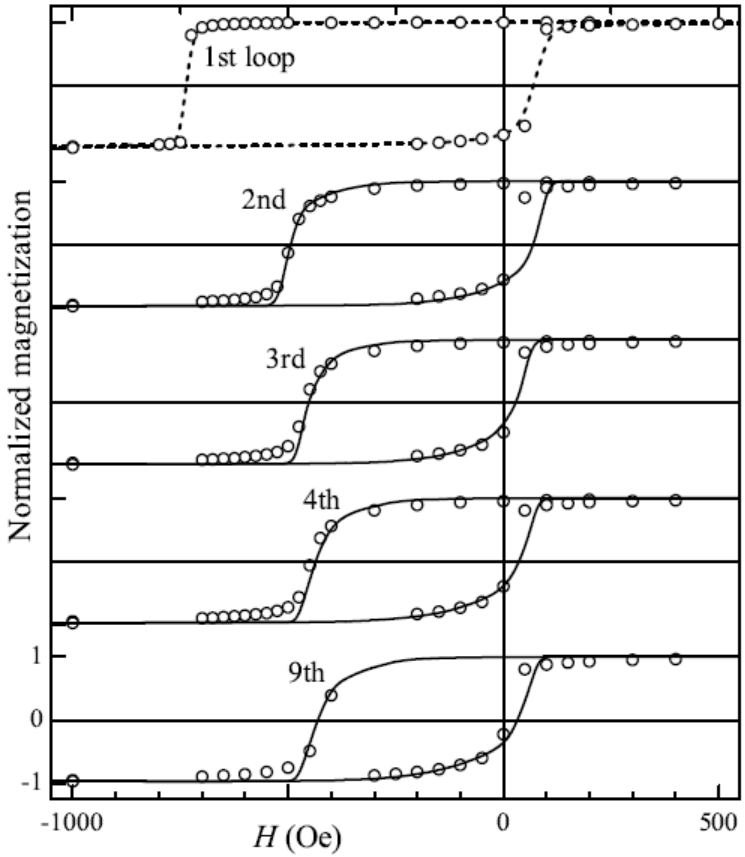

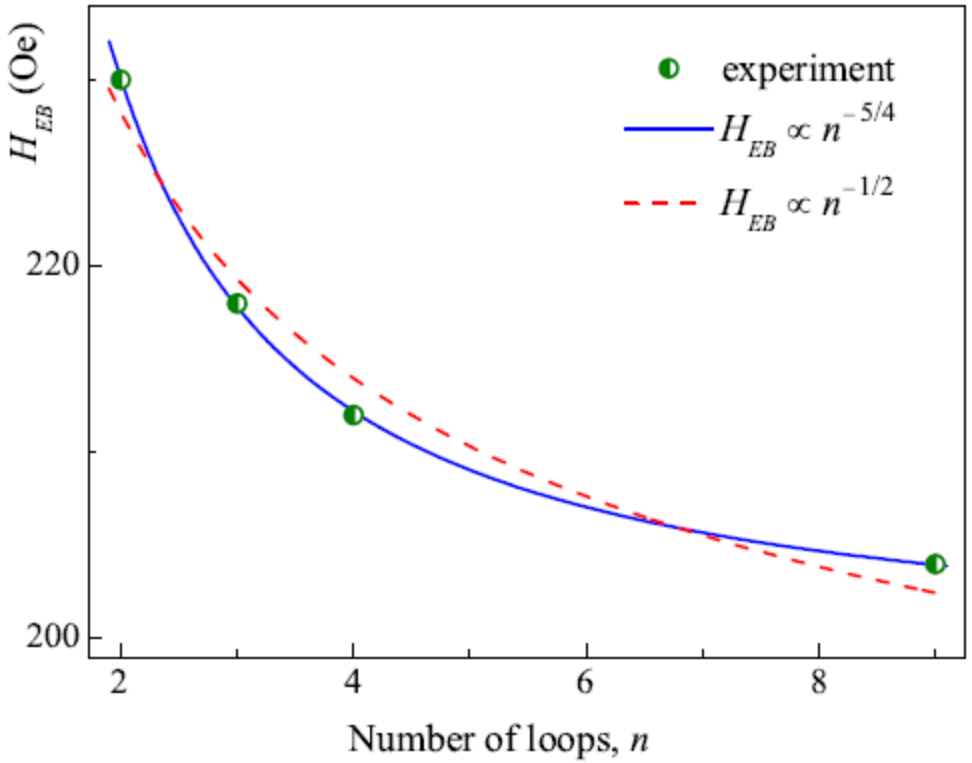

Training effect of H_{EB} versus n for $n > 1$ (symbols). The solid and dashed lines represent the best-fitting curves calculated using $H_{EB}(n) = H_{EB}(\infty) + k/n^r$ for $r = 5/4$ and $1/2$, respectively.

EB and Ferromagnetic Resonance (FMR):

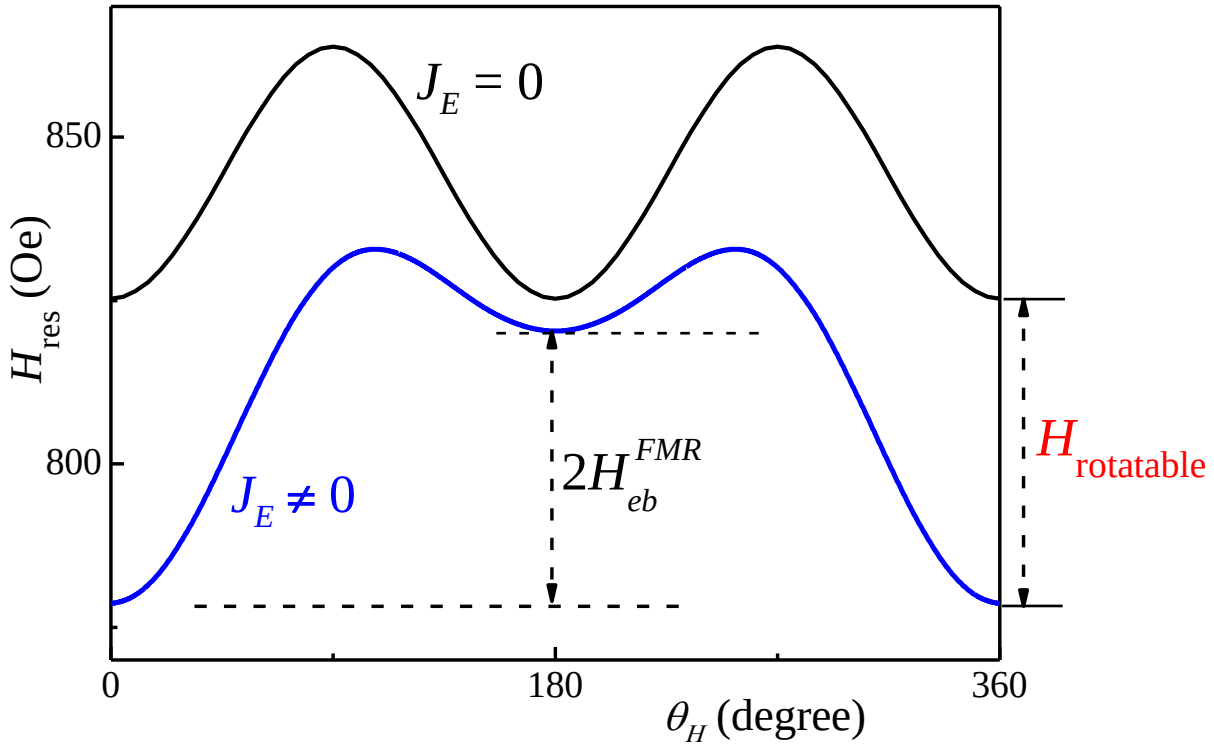

- Different H_{res} values at $\theta_H = 0^o$ and 180^o
- Isotropic shift in H_{res} vs. θ_H.

Initializing the EB:

Application of **H**

- ✓ **H** very strong at the measurement *T*
- ✓ during deposition
- ✓ post-deposition
  - ➢ annealing
  - ➢ ion irradiation

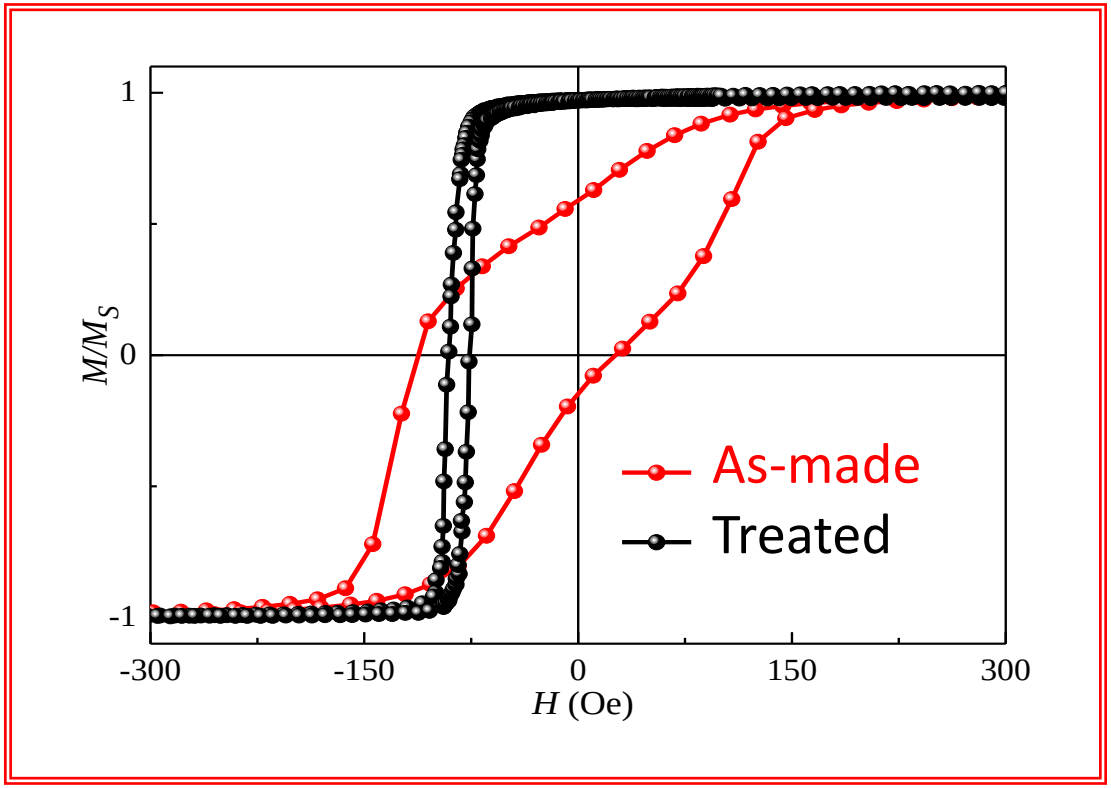

✓ FMR: aannealed samples

IrMn / Cr / Co film

PHYSICAL REVIEW B **85**, 224438 (2012)

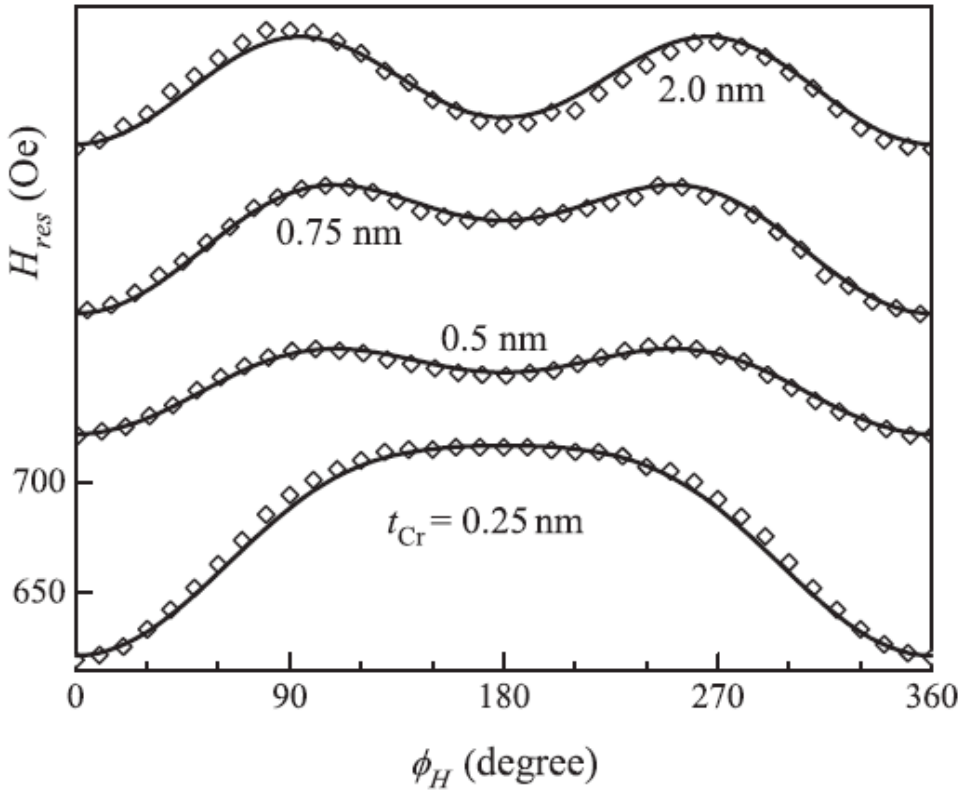

H_W = 510 Oe

M_S = 1400 emu/cm^3

ω/γ = 3.497 kOe

t_{Cr} (nm)	J (erg/cm^2)	H_U (Oe)	H_{RA} (Oe)
0.25	0.033±0.001	15±1	− 11±1
0.5	0.009±0.001	12±1	− 27±1
0.75	0.014±0.001	18±1	− 53±1
1.0	0.013±0.001	18±1	− 44±1
1.5	0.008±0.001	25±1	− 50±1
2.0	0.004±0.001	22±1	− 59±1

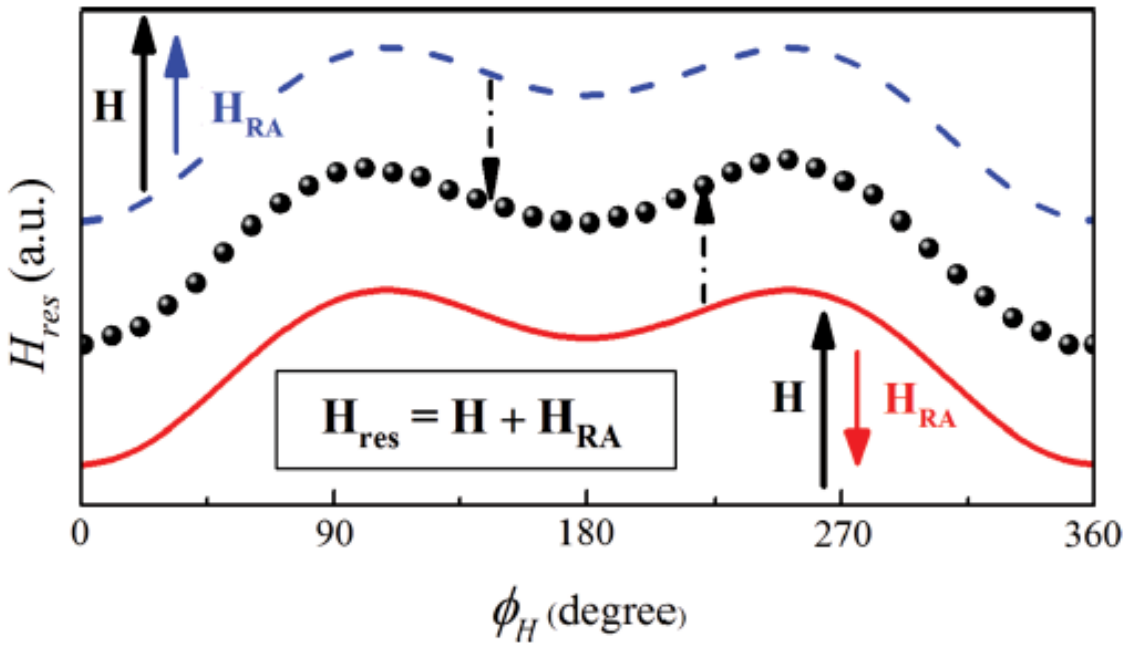

Experimental (symbols) and model $H_{res}(\phi_H)$ curves simulated without taking into account the rotatable anisotropy. The dashed line represents the $\mathbf{H} \parallel \mathbf{H_{RA}}$ case when the fitting curve must be shifted downward. For antiparallel $\mathbf{H}$ and $\mathbf{H_{RA}}$, the shift is upward (solid curve).

PHYSICAL REVIEW B **85**, 224438 (2012)

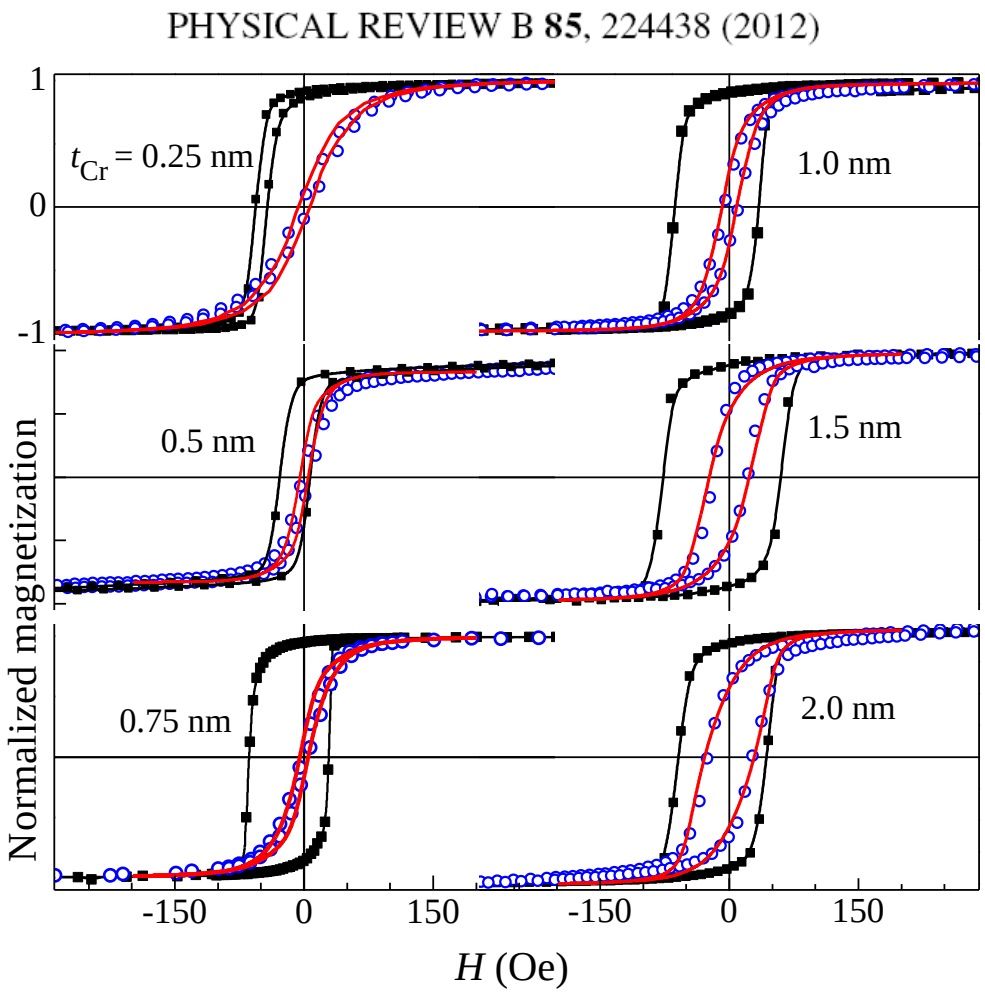

FMR seems to be a better tool for RA estimation:

- **practically saturated samples;**
- **it isn't necessary to know the AF anisotropy type;**
- **gives the sign of the coupling.**

Recent unpublished results: negative RA in IrMn/NiFe films

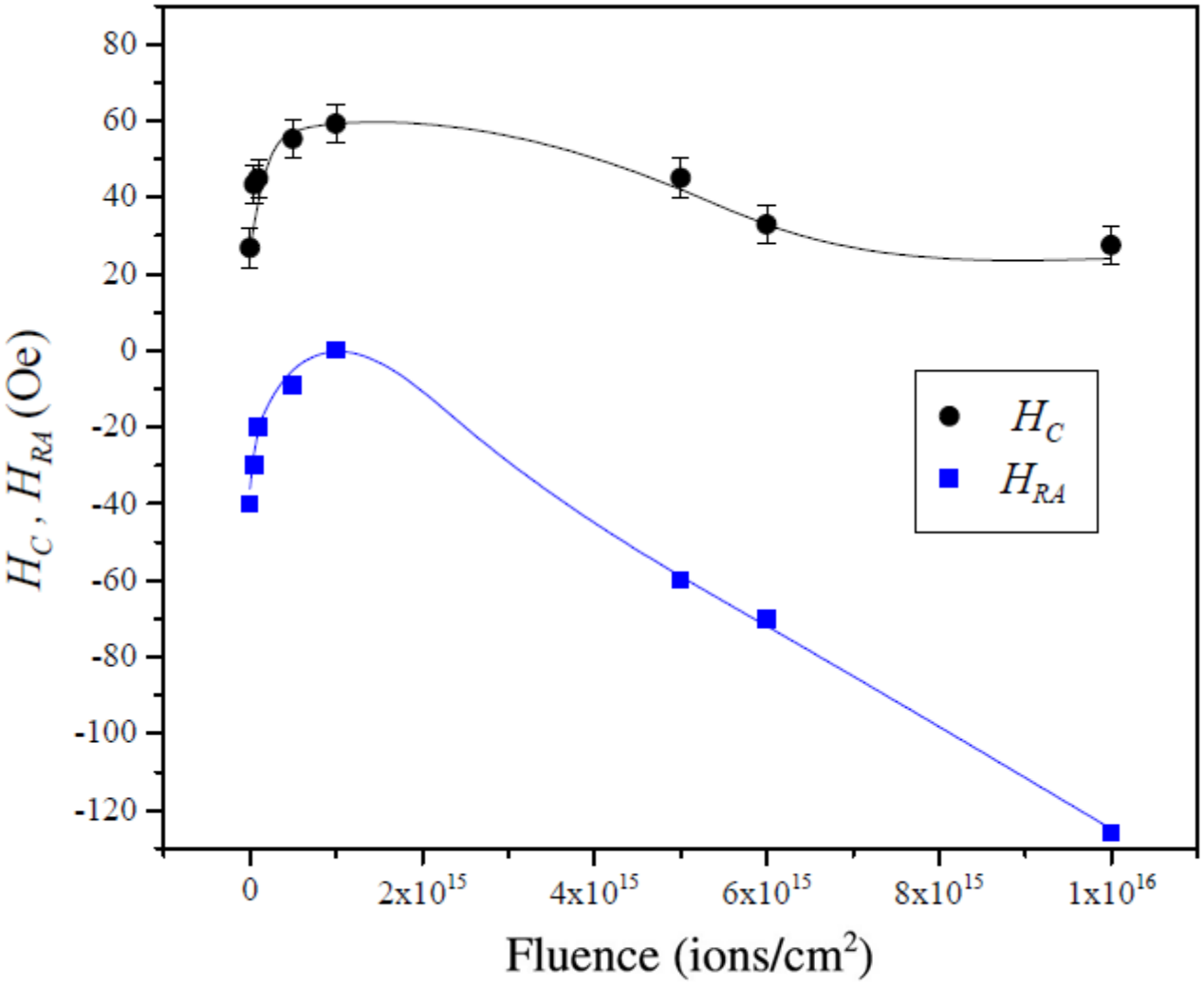

Journal of Magnetism and Magnetic Materials 346 (2013) 1–4

Contents lists available at SciVerse ScienceDirect

Journal of Magnetism and Magnetic Materials

journal homepage: www.elsevier.com/locate/jmmm

Rotatable anisotropy of $Ni_{81}Fe_{19}/Ir_{20}Mn_{80}$ films: A study using broadband ferromagnetic resonance

R. Dutra [a], D.E. Gonzalez-Chavez [a], T.L. Marcondes [a], A.M.H. de Andrade [b], J. Geshev [b], R.L. Sommer [a,*]

Other names for the RA can be found, e.g.,
AF-induced canted uniaxial anisotropy
J. McCord, C. Hamann, R. Schäfer, L. Schultz, and R. Mattheis, Phys. Rev. B 78, 094419 (2008).

Thermal dependence of H_{iso}

Thesis: FRANCISCARLOS GOMES DA SILVA

Core/shell particles: H_{iso} does not depend on the texture of the sample or on the orientation of H_{ext}

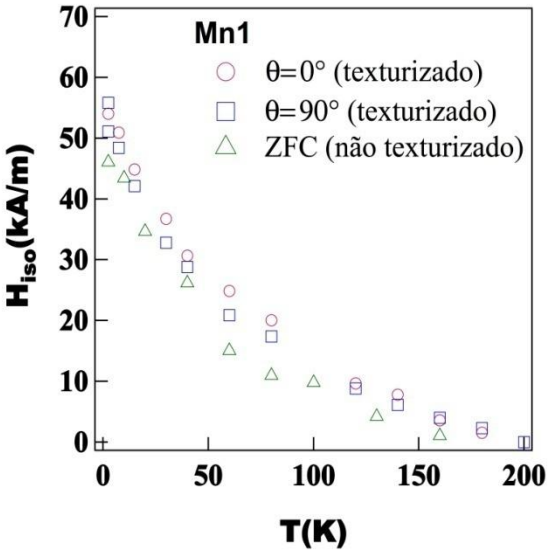

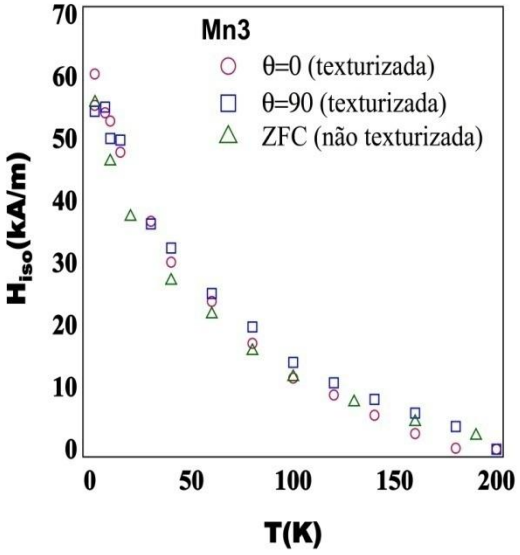

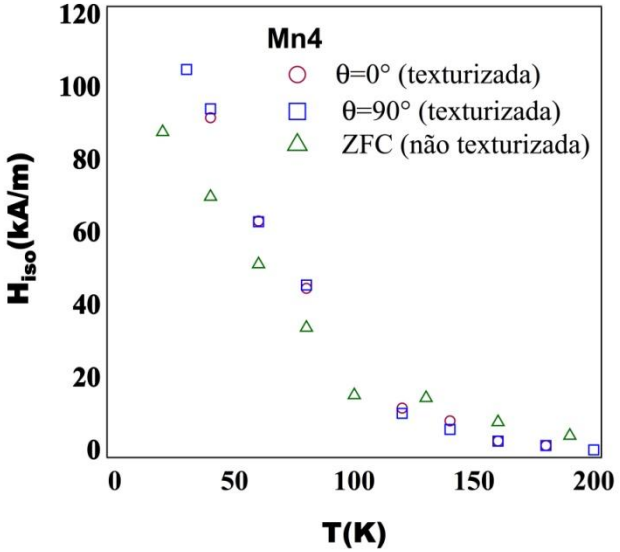

At 9.26 GHz, this unidirectional field H_{iso} can be identified as a dynamical exchange anisotropy field coming from surface spins

V. Shilov et al., Phys. Rev. B **60** (1999) 11902

F. Gazeau et al., J. Magn. Magn. Mat. **186** (1998) 175-187)

Sistemas de mais de uma fase magnética: simulações são necessárias!

Mas cuidado com isso!

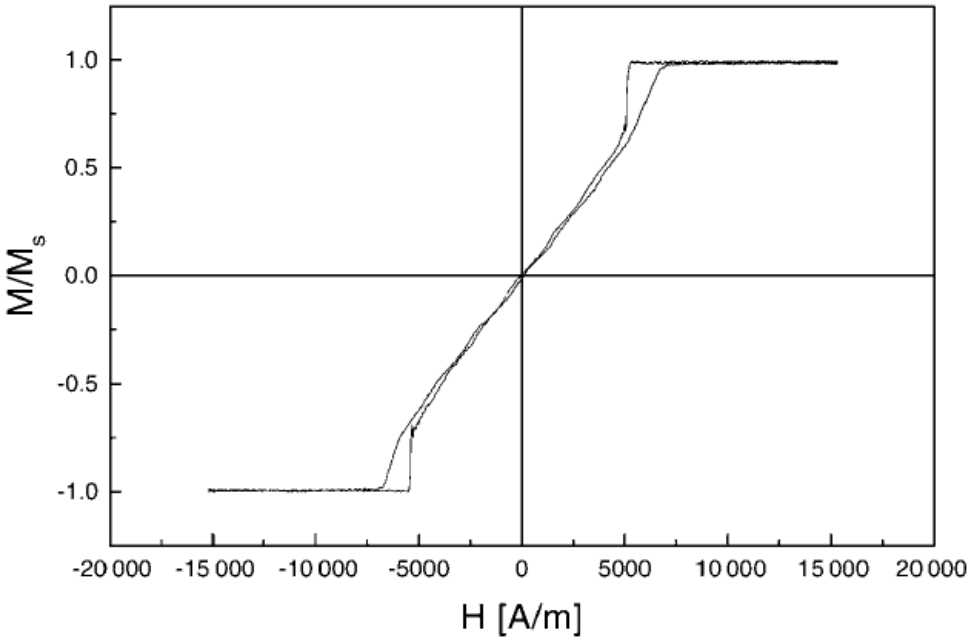

J. Phys. D: Appl. Phys. **34** (2001) 48–53

Interpretação: movimento de paredes de domínio

Rotação coerente

ou

movimento de paredes de domínio?

ou

dinâmica de vórtices magnéticos?

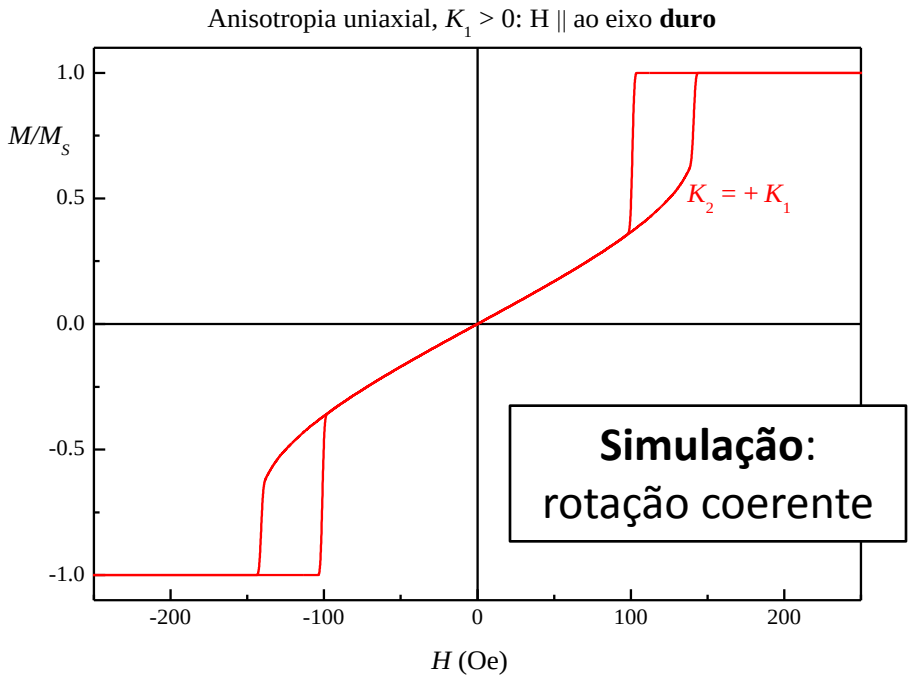

Simulação: rotação coerente

Remanence plots

Classical symmetric loops (no EB):

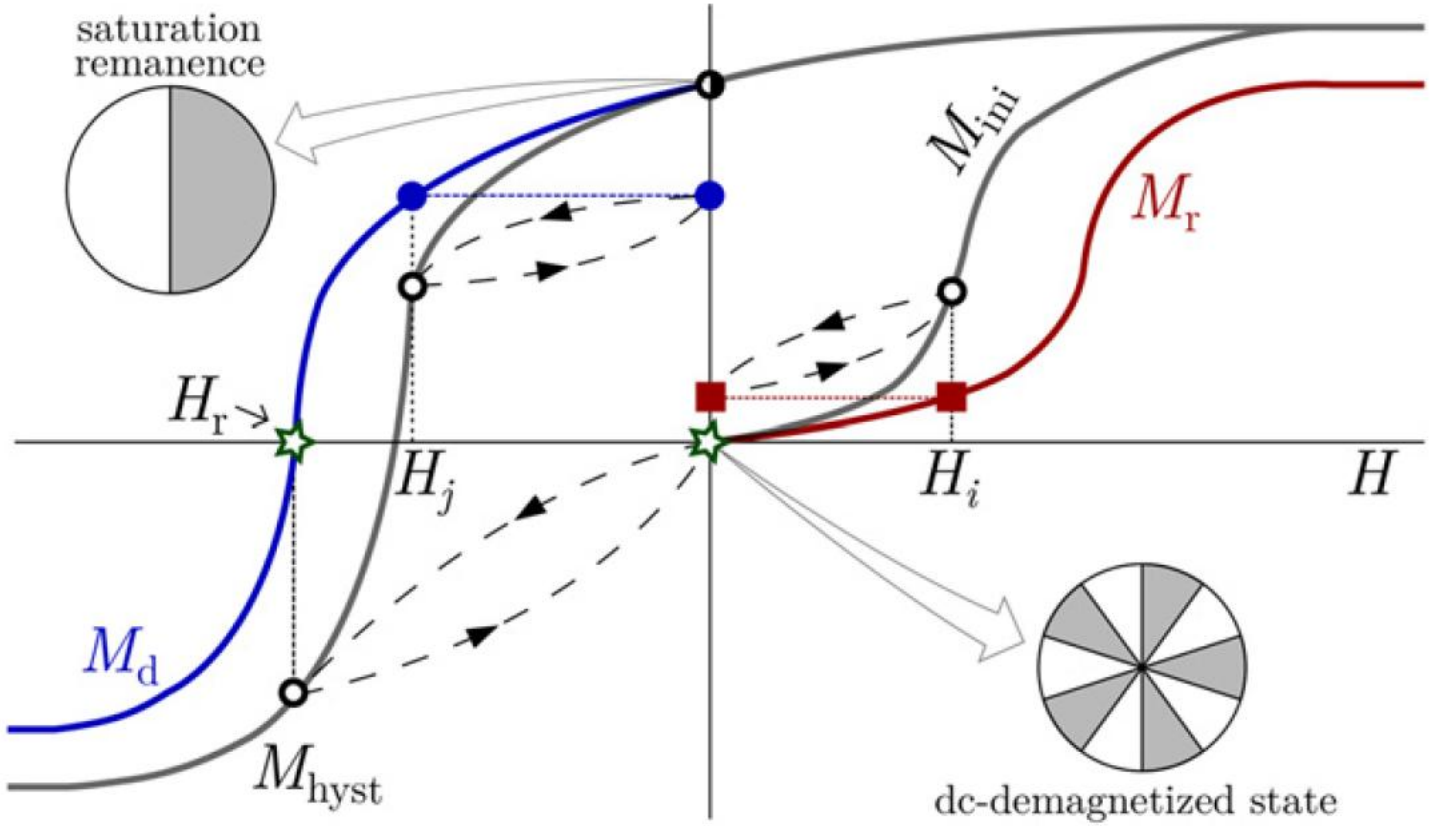

R. Cichelero, A. Harres, K.D. Sossmeier, J.E. Schmidt, and J. Geshev, "Magnetic interactions in **exchange-coupled yet unbiased** IrMn/NiCu bilayers," Journal of Physics: Condensed Matter **25** (2013) 426001.

Remanence plots

$m_r \times m_d$?

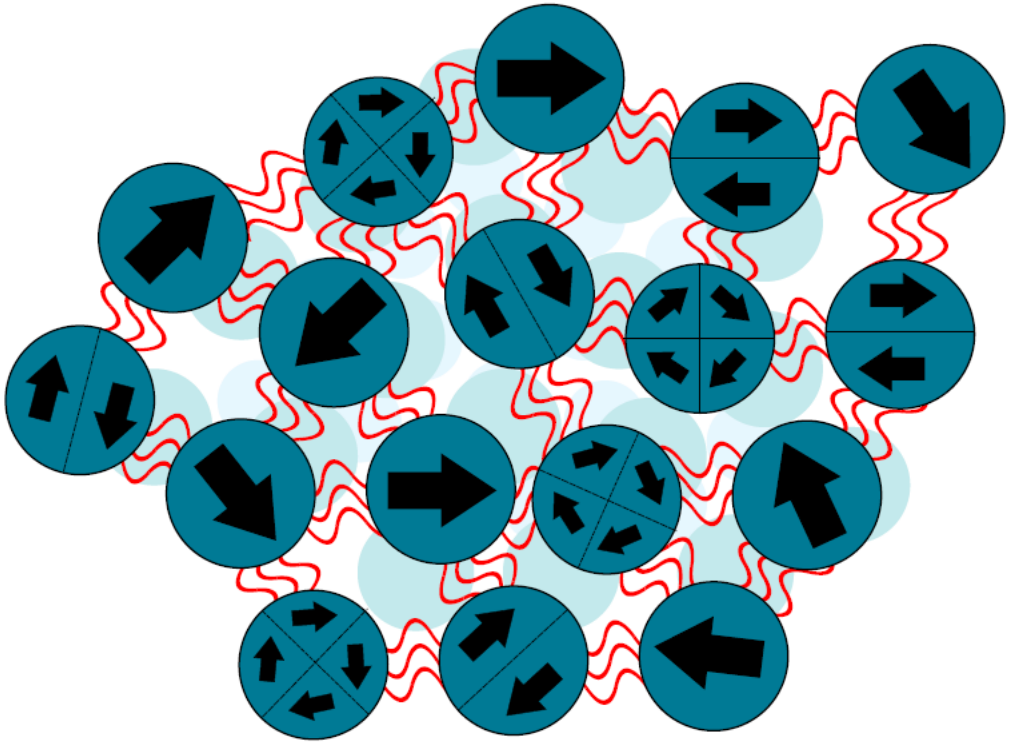

Remanence plots

$m_r \times m_d$?

- Não-interagentes
- mono-domínios
- anisotropia uniaxial

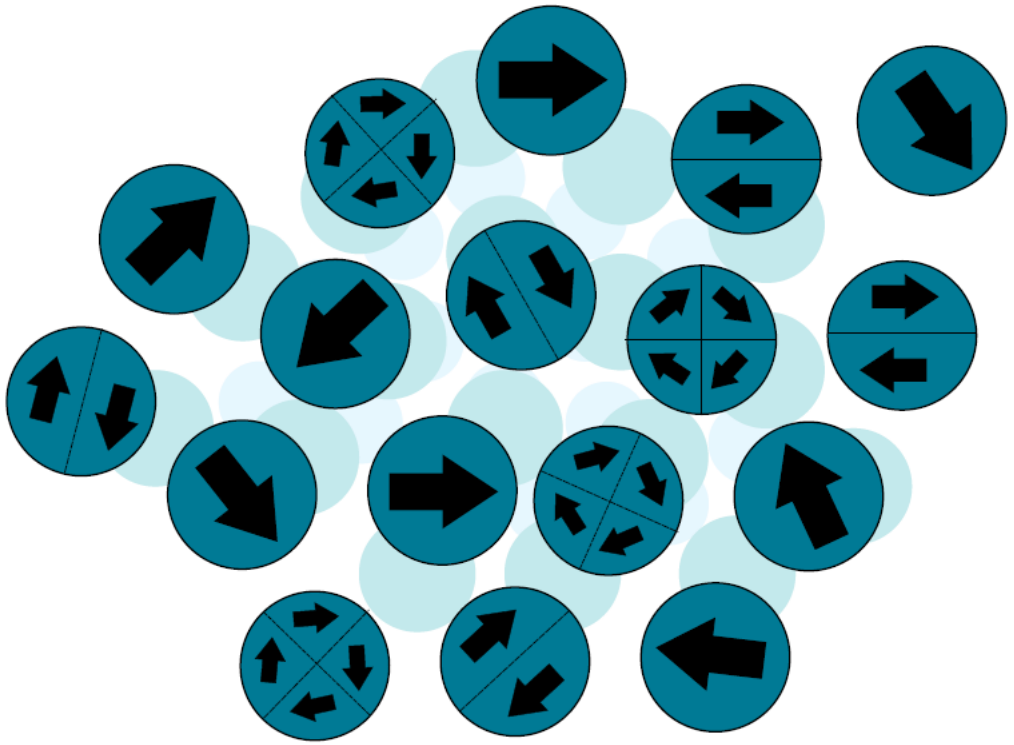

Remanence plots

$m_r \times m_d$?

- Não-interagentes
- mono-domínios
- anisotropia uniaxial

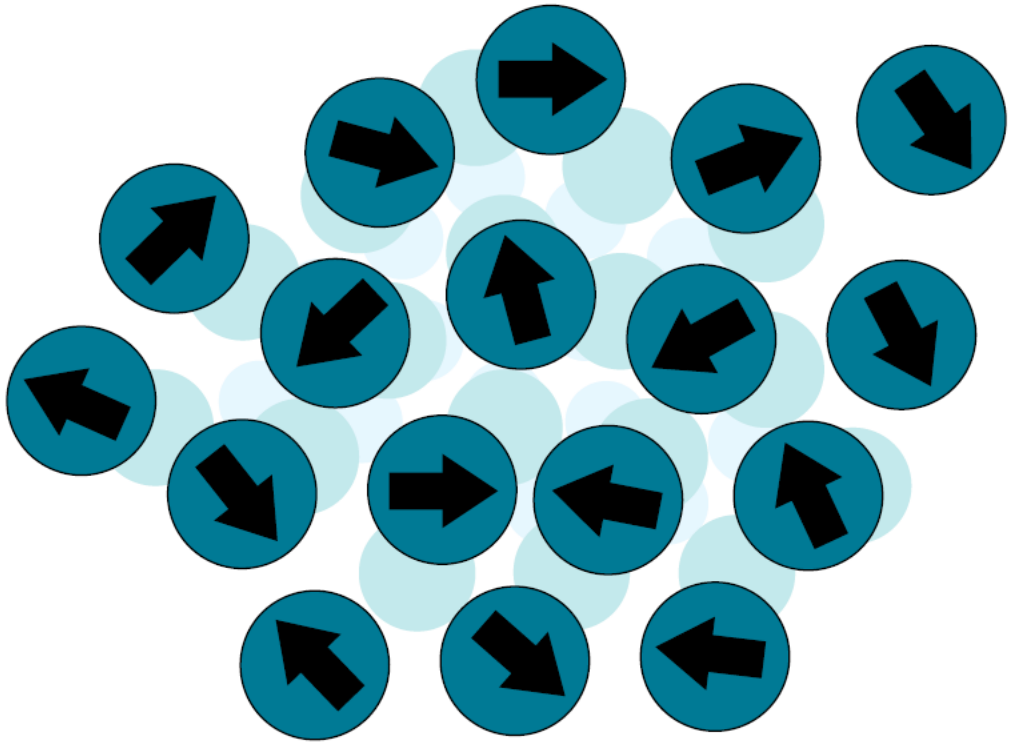

Remanence plots

$m_r \times m_d$?

- Não-interagentes
- mono-domínios
- anisotropia uniaxial

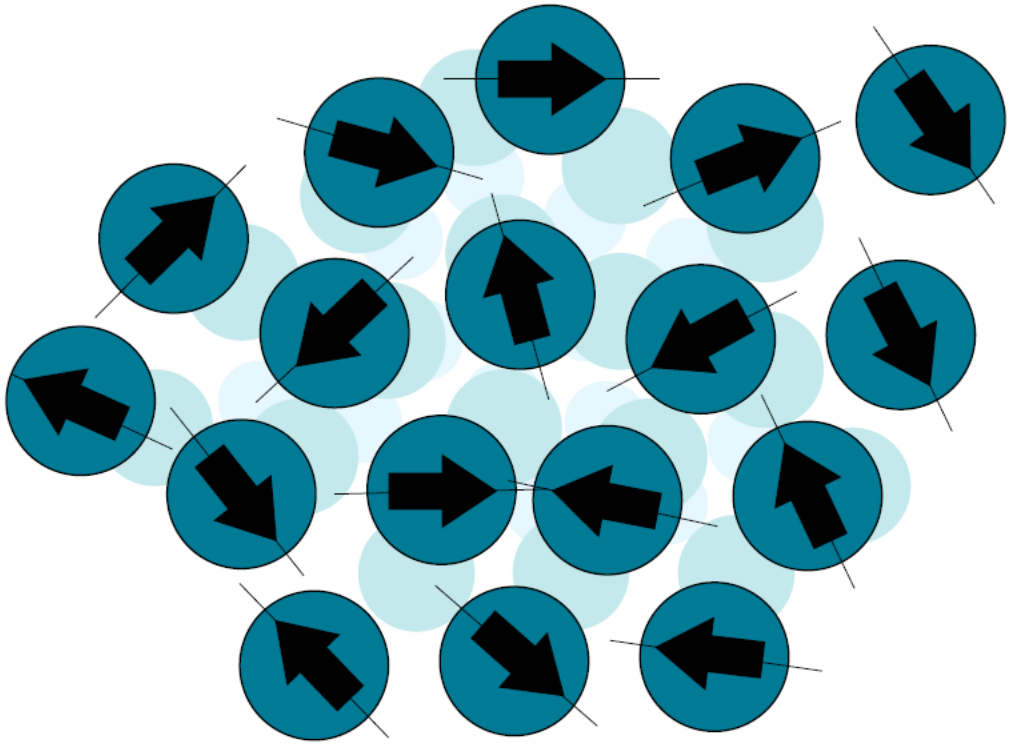

Remanence plots

$m_r \times m_d \implies$ **Henkel plots**

Partículas não-interagentes, mono-domínios, anisotropia uniaxial

$$m_d(H) = 1 - 2m_r^{ac}(H)$$

$$m_r^{dc}(H) = 1 - m_d(H) \quad \text{para} \quad H < H_r$$
$$m_r^{dc}(H) = 1 \quad \text{para} \quad H \geq H_r$$

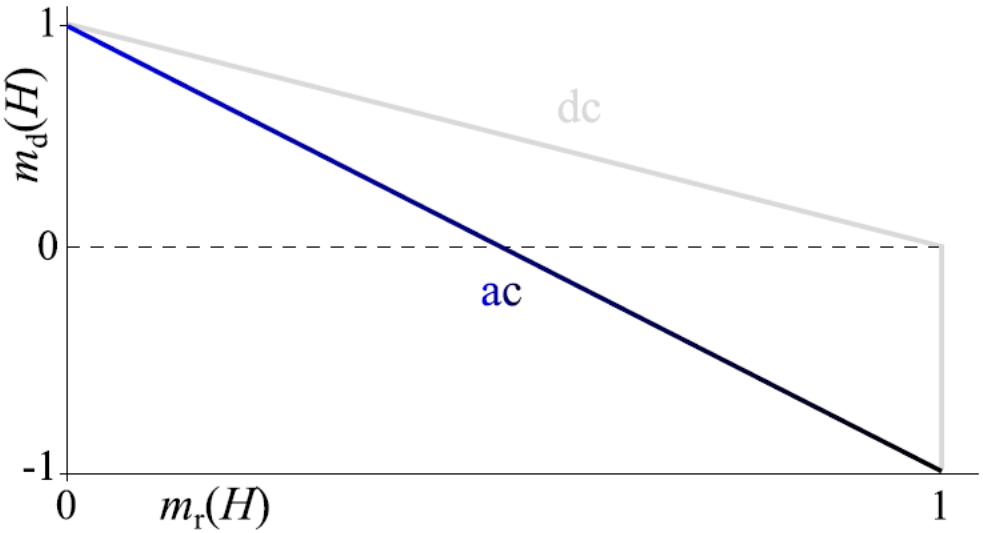

Remanence plots

Desvios

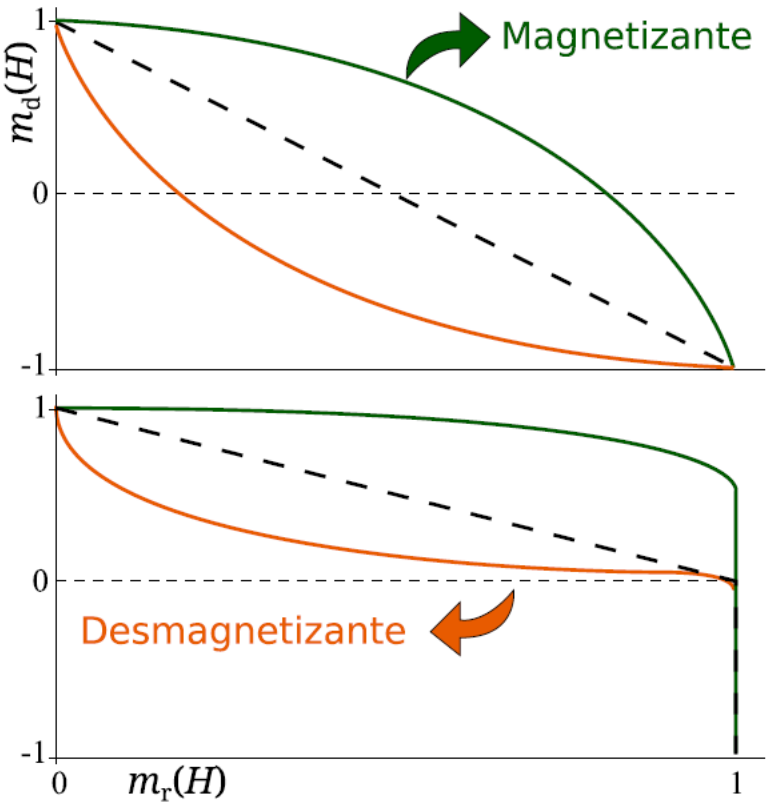

Remanence plots

$m_r \times m_d \implies$ **Henkel plots**

Partículas não-interagentes, mono-domínios, anisotropia uniaxial

$$m_d(H) = 1 - 2m_r^{ac}(H)$$

$$m_r^{dc}(H) = 1 - m_d(H) \quad \text{para} \quad H < H_r$$
$$m_r^{dc}(H) = 1 \quad \text{para} \quad H \geq H_r$$

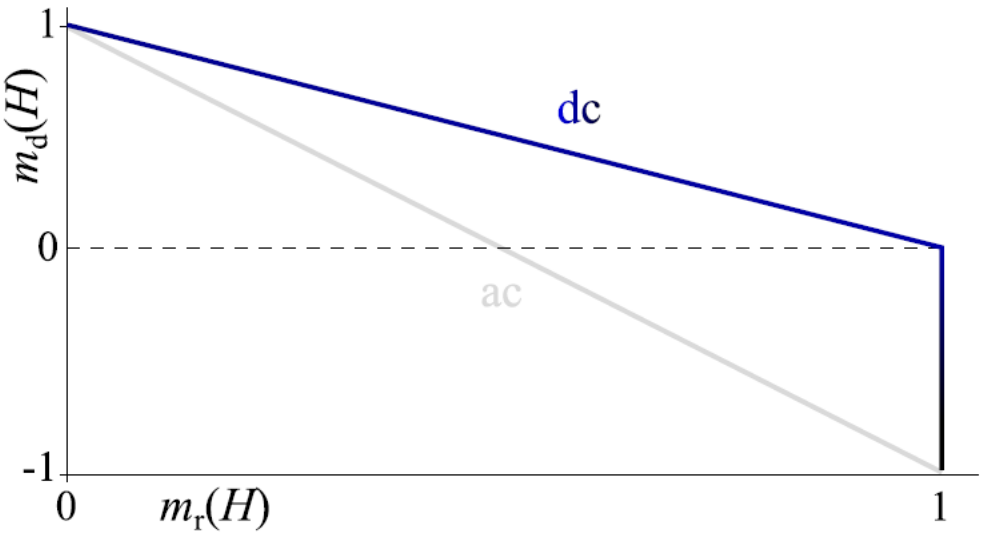

Remanence plots

$$m_r \times m_d \implies \delta M$$

$$\delta M(H) = 2m_r^{ac}(H) - 1 + m_d(H)$$

$$\delta M(H) = m_r^{dc}(H) - 1 + m_d(H) \quad \text{para} \quad H < H_r$$
$$\delta M(H) = m_r^{dc}(H) - 1 \quad \text{para} \quad H \geq H_r$$

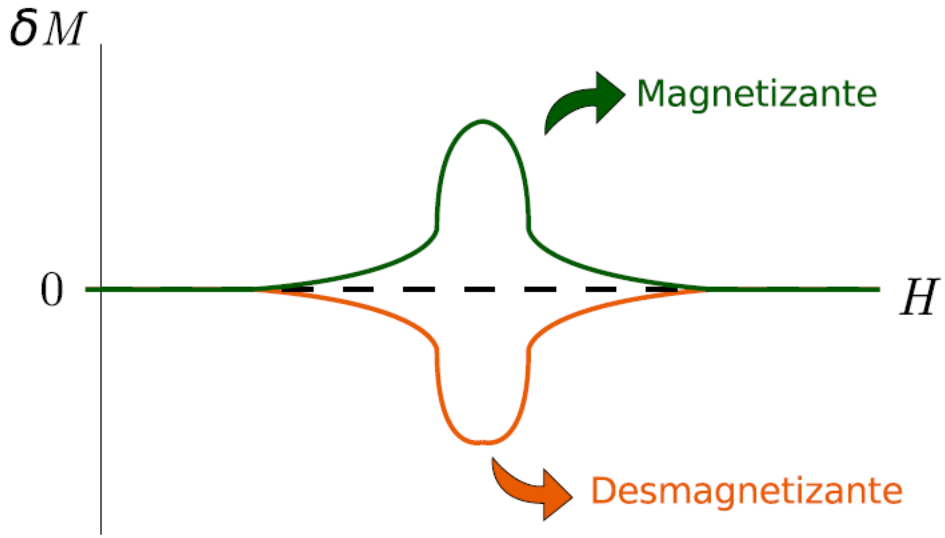

P. Mayo *et al.*, *IEEE Trans. Magn.*, vol. 25, p. 3881, 1989.

NiCu/IrMn unbiased bilayers

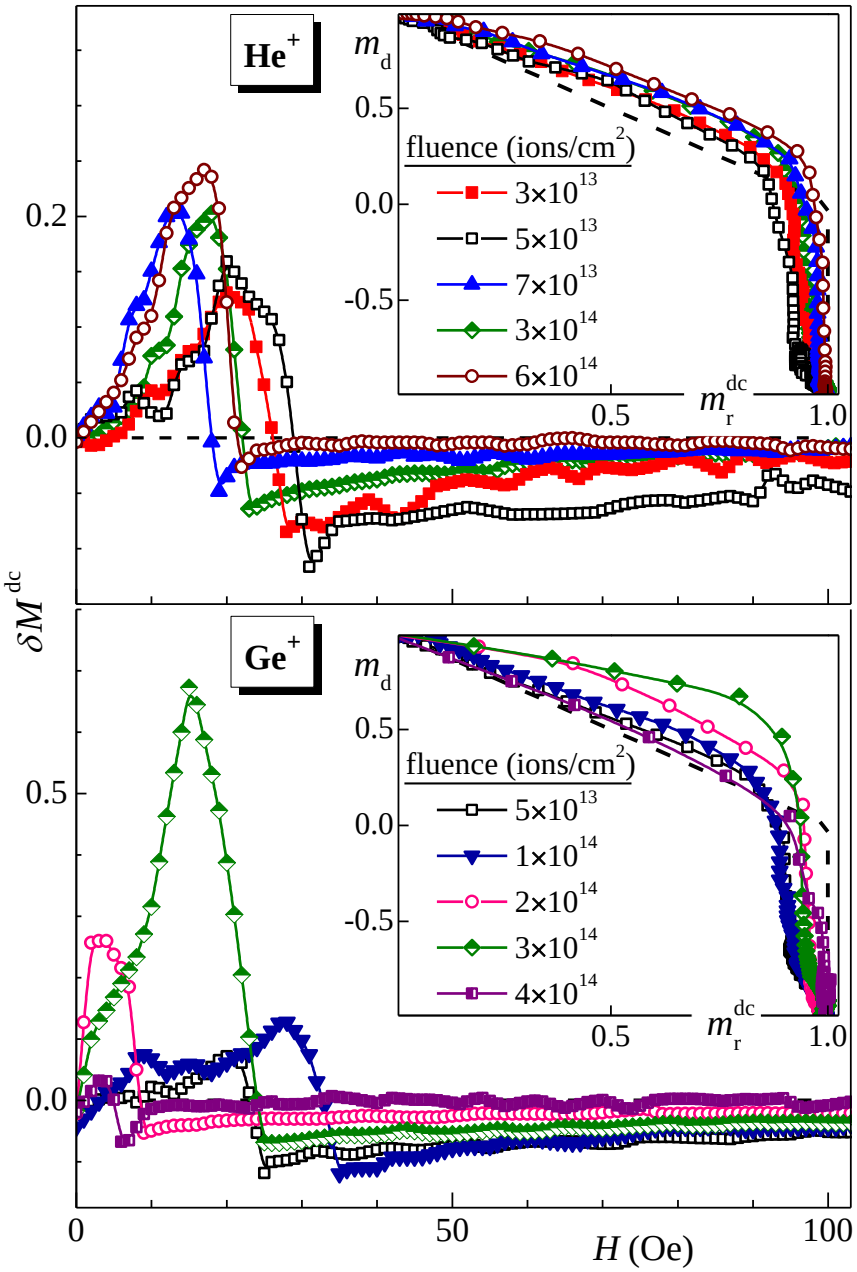

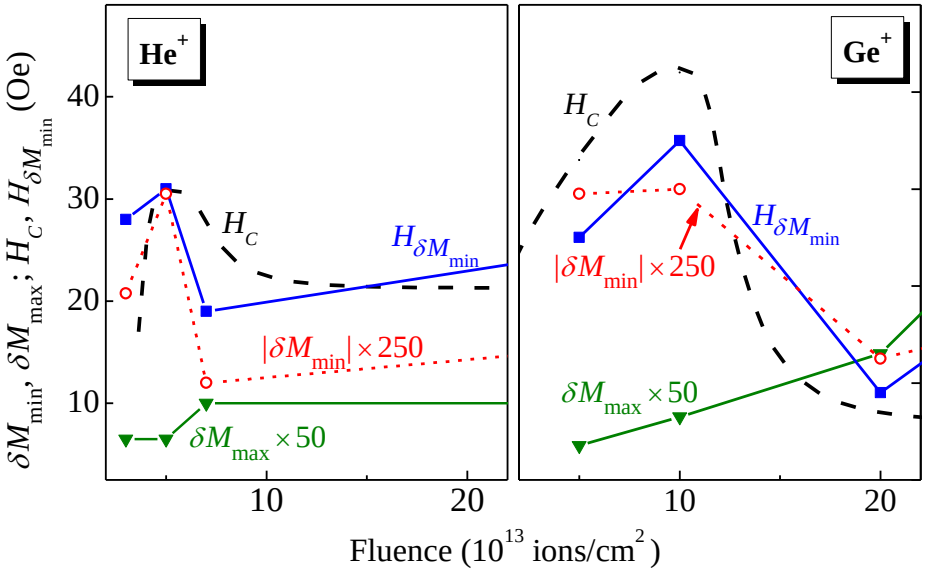

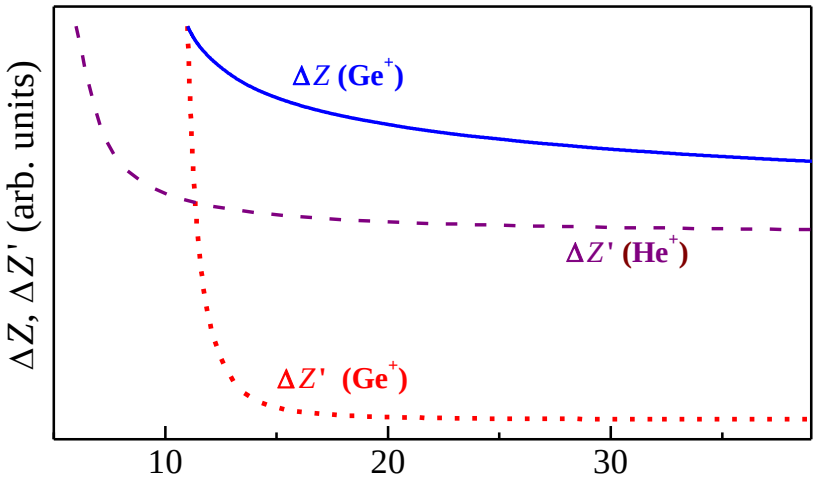

$$H_C \propto \sqrt{Z'/Z}$$

S. Zhang, D.V. Dimitrov, G.C. Hadjipanayis, J.W. Cai, and C.L. Chien, JMMM **198-199**, 468 (1999).

Numerical simulations based on Landau-Lifshitz-Gilbert (LLG) equation

$$\frac{d\mathbf{M}}{dt} = -\frac{\gamma}{1+\alpha^2}\left(\mathbf{M}\times\mathbf{H}_{\mathrm{ef}}\right) - \frac{\gamma\alpha}{(1+\alpha^2)M_s}\mathbf{M}\times\left(\mathbf{M}\times\mathbf{H}_{\mathrm{ef}}\right)$$

$$\mathbf{H}_{\mathrm{ef}} = \mathbf{H}_{\mathrm{ap}} + \mathbf{H}_{\mathrm{anis}} + \mathbf{H}_{\mathrm{ex}} + \mathbf{H}_{\mathrm{dip}}$$

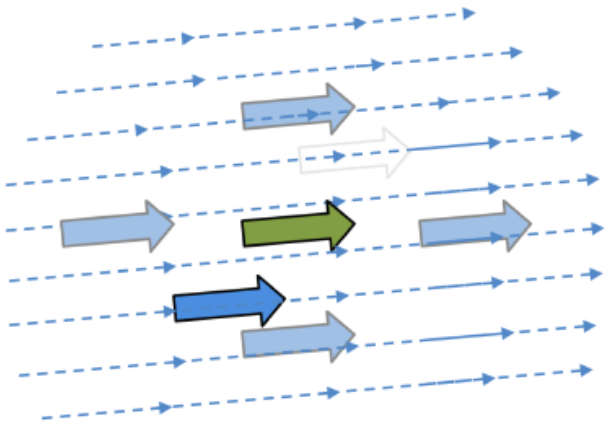

Campo aplicado

$$\mathbf{H}_{\mathrm{ap}} = \mathbf{H}$$

Numerical simulations based on Landau-Lifshitz-Gilbert (LLG) equation

$$\frac{d\mathbf{M}}{dt} = -\frac{\gamma}{1+\alpha^2}\left(\mathbf{M}\times\mathbf{H}_{\mathrm{ef}}\right) - \frac{\gamma\alpha}{(1+\alpha^2)M_s}\mathbf{M}\times\left(\mathbf{M}\times\mathbf{H}_{\mathrm{ef}}\right)$$

$$\mathbf{H}_{\mathrm{ef}} = \mathbf{H}_{\mathrm{ap}} + \mathbf{H}_{\mathrm{anis}} + \mathbf{H}_{\mathrm{ex}} + \mathbf{H}_{\mathrm{dip}}$$

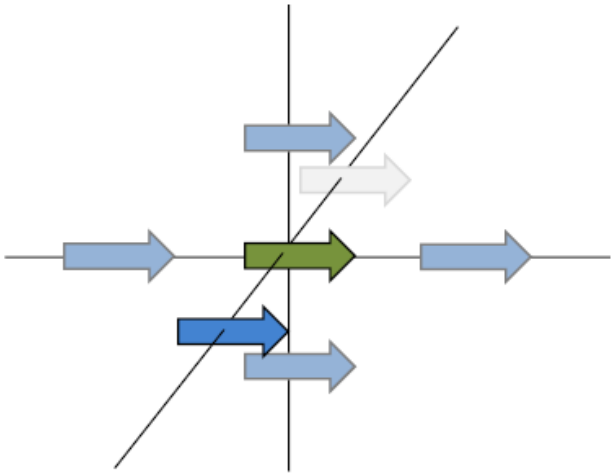

Anisotropia uniaxial

$$\mathbf{H}_{\mathrm{anis}} = \mathbf{H}_{\mathrm{uni}} = \frac{2KV}{M_s}\left(\mathbf{M}\cdot\mathbf{p}\right)\mathbf{p}$$

Numerical simulations based on Landau-Lifshitz-Gilbert (LLG) equation

$$\frac{d\mathbf{M}}{dt} = -\frac{\gamma}{1+\alpha^2}(\mathbf{M}\times\mathbf{H}_{\mathrm{ef}}) - \frac{\gamma\alpha}{(1+\alpha^2)M_s}\mathbf{M}\times(\mathbf{M}\times\mathbf{H}_{\mathrm{ef}})$$

$$\mathbf{H}_{\mathrm{ef}} = \mathbf{H}_{\mathrm{ap}} + \mathbf{H}_{\mathrm{anis}} + \mathbf{H}_{\mathrm{ex}} + \mathbf{H}_{\mathrm{dip}}$$

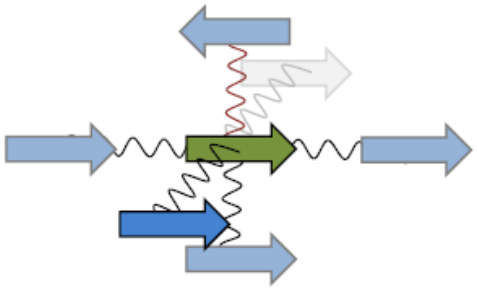

Interação de troca

$$\mathbf{H}_{\mathrm{ex}} = \frac{j}{M_{\mathrm{s}}\, t_{\mathrm{M}}}\mathbf{M}'$$

Numerical simulations based on Landau-Lifshitz-Gilbert (LLG) equation

$$\frac{d\mathbf{M}}{dt} = -\frac{\gamma}{1+\alpha^2}\left(\mathbf{M}\times\mathbf{H}_{\mathrm{ef}}\right) - \frac{\gamma\alpha}{(1+\alpha^2)M_s}\mathbf{M}\times\left(\mathbf{M}\times\mathbf{H}_{\mathrm{ef}}\right)$$

$$\mathbf{H}_{\mathrm{ef}} = \mathbf{H}_{\mathrm{ap}} + \mathbf{H}_{\mathrm{anis}} + \mathbf{H}_{\mathrm{ex}} + \mathbf{H}_{\mathrm{dip}}$$

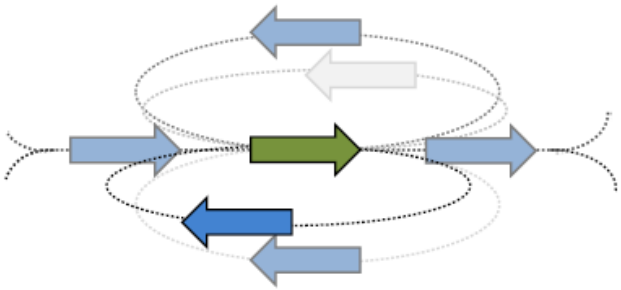

Interação dipolar

$$\mathbf{H}_{\mathrm{dip}} = -\frac{V'\mathbf{M}'}{R^3} + \frac{3V'\left(\mathbf{M}'\cdot\hat{e}\right)\hat{e}}{R^3}$$

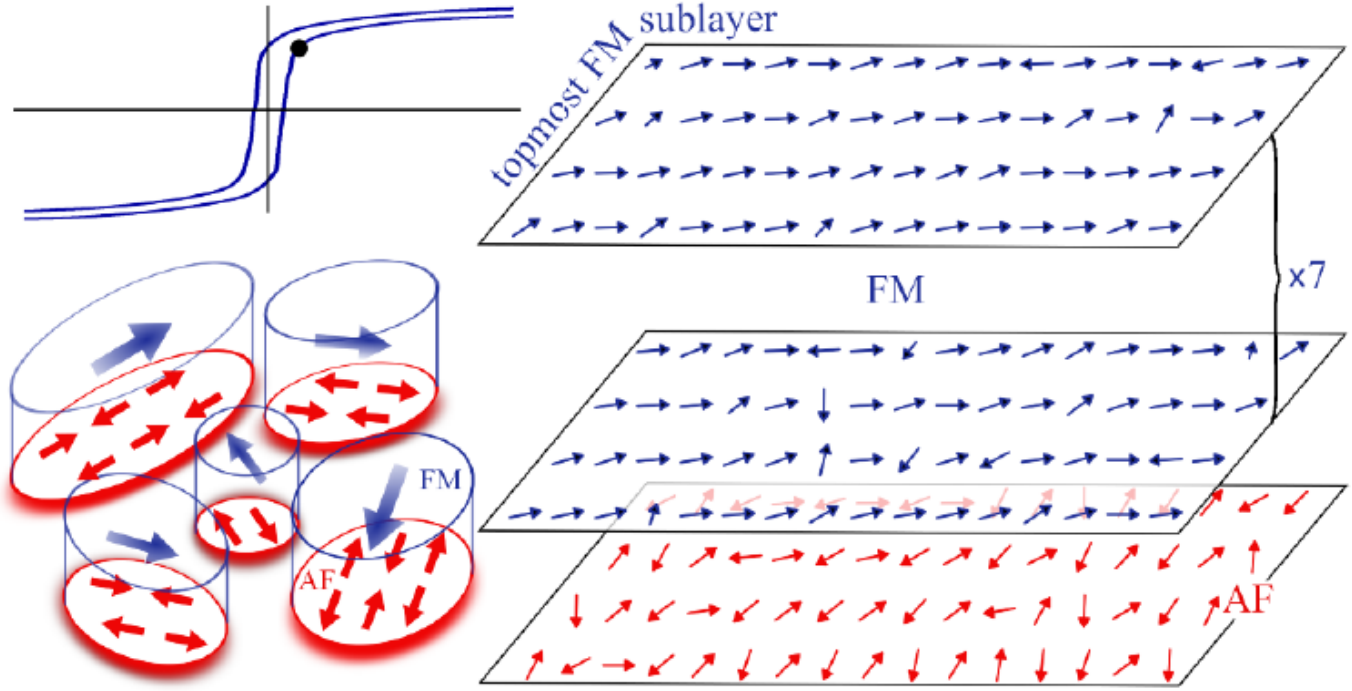

Schematic representation of the AF/FM granular system showing the AF spin planes in the interfacial region of each grain. Top left: Low-field region of a simulated hysteresis loop.

R. Cichelero, A. Harres, K.D. Sossmeier, J.E. Schmidt, and J. Geshev, "Magnetic interactions in exchange-coupled yet unbiased IrMn/NiCu bilayers," Journal of Physics: Condensed Matter **25** (2013) 426001.

Exchange-coupled yet unbiased bilayer

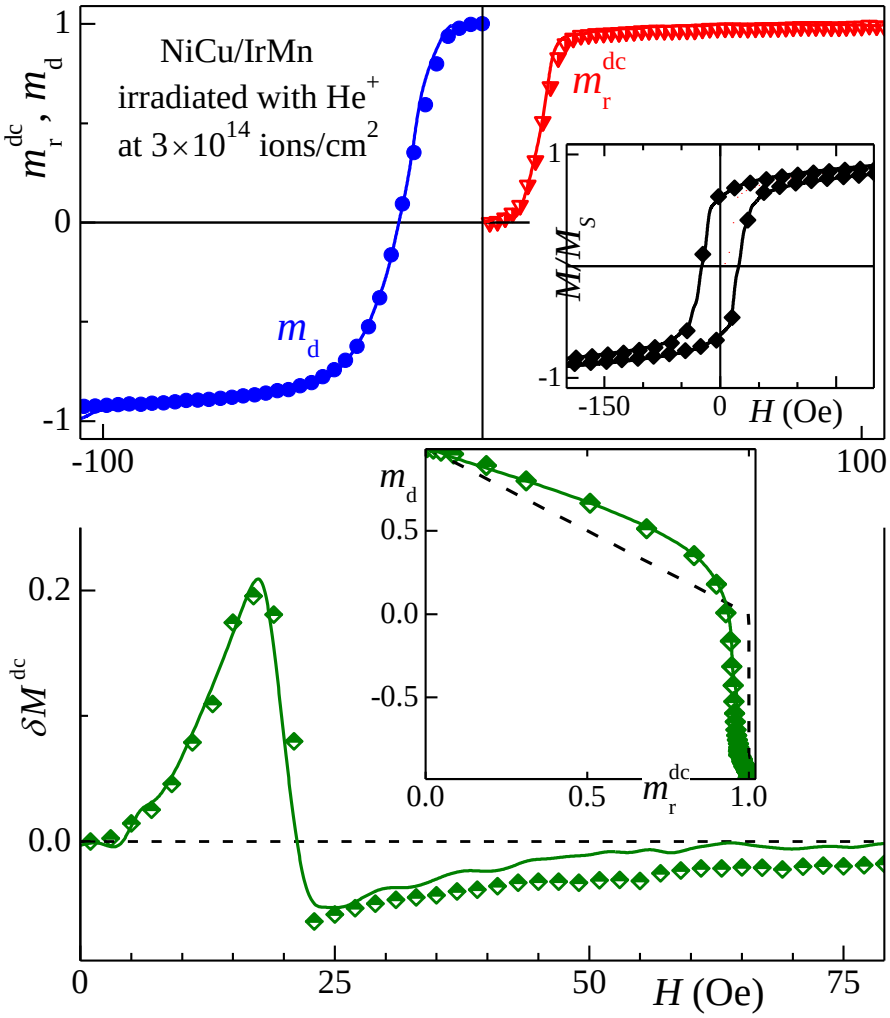

R. Cichelero, A. Harres, K.D. Sossmeier, J.E. Schmidt, and J. Geshev, "Magnetic interactions in exchange-coupled yet unbiased IrMn/NiCu bilayers," Journal of Physics: Condensed Matter **25** (2013) 426001.

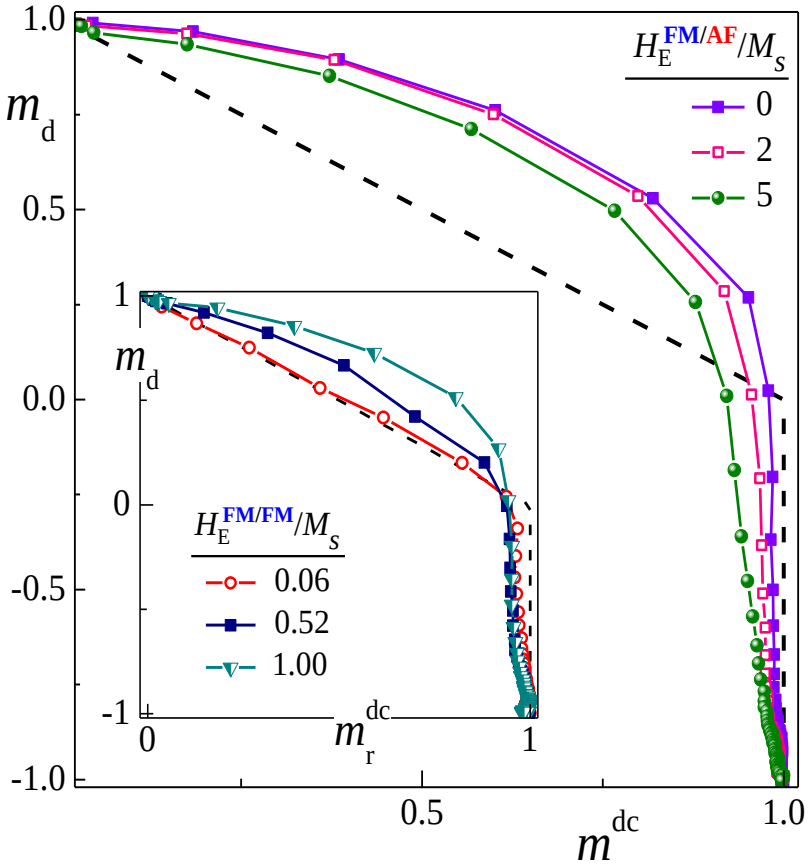

Henkel plots simulated varying the FM/AF coupling for constant $H_E^{FM/FM}/M_s = 1$ and varying the FM/FM coupling when $H_E^{AF/FM}/M_s = 5$ (inset). The other parameters used are $H_U^{FM}/M_s = 9$ and $H_U^{AF}/M_s = 33$ as mean values with standard deviations 0.3 and 3, respectively, and $H_E^{AF/AF}/M_s = 50$.

R. Cichelero, A. Harres, K.D. Sossmeier, J.E. Schmidt, and J. Geshev, "Magnetic interactions in exchange-coupled yet unbiased IrMn/NiCu bilayers," Journal of Physics: Condensed Matter **25** (2013) 426001.

Remanence plots

Asymmetric, biased loops: not easy to define H_{eb} and H_C:

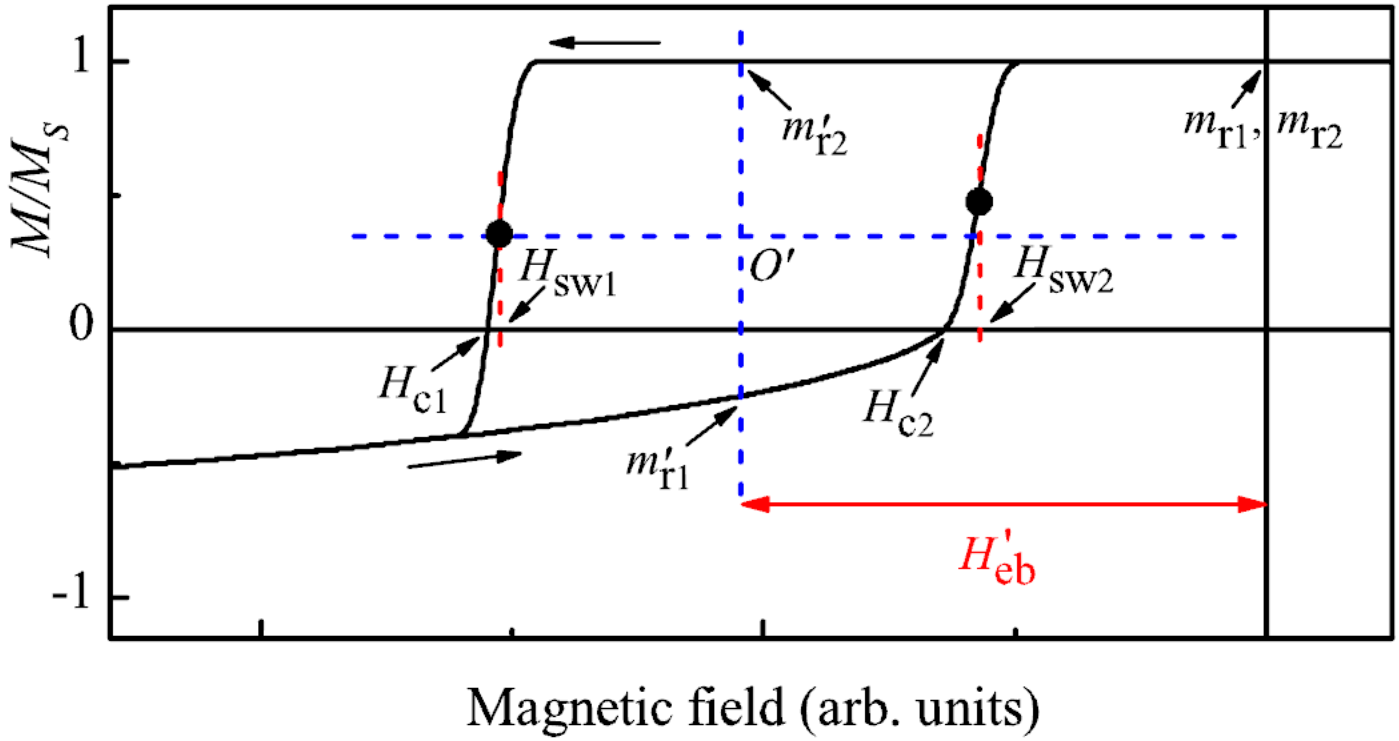

Scheme representing the parameters used in the characterization of exchange-bias systems. The arrows indicate the directions of the magnetic field sweeps.

A. Harres, R. Cichelero, L. G. Pereira, J. E. Schmidt, and J. Geshev, "Remanence plots technique extended to exchange bias systems," Journal of Applied Physics **114** (2013) 043902.

Biased asymmetric loops (EB):

m_r & m_d - Co/IrMn

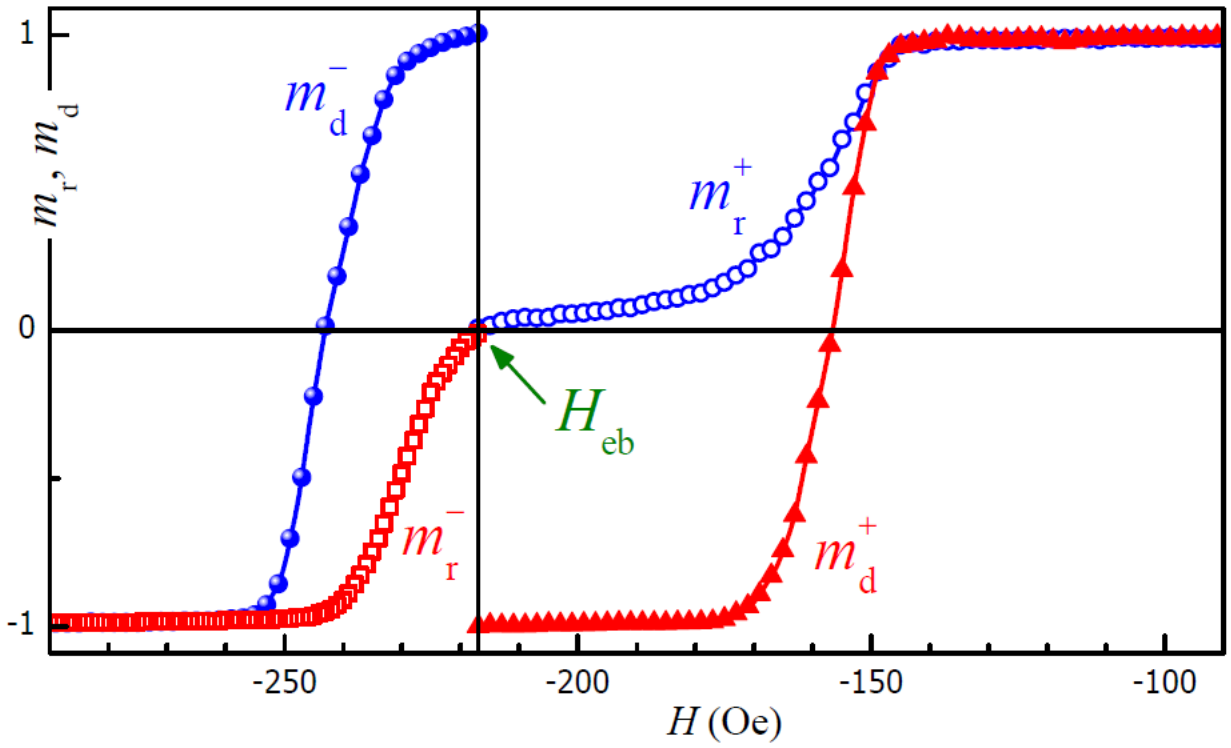

Asymmetric loops: there are two distinct IRM curves, m_r^{dc+} and m_r^{dc-}, and two DCD: m_d^+ and m_d^+.

Biased asymmetric loops (EB):

$$\delta M(H) = 2m_r(H) - 1 + 2m_d(H).$$

$$\delta M^{dc}(H) = m_r^{dc}(H) - 1 + m_d(H) \quad \text{for} \quad H < H_r$$

$$\text{and} \qquad = m_r^{dc}(H) - 1 \qquad \text{for} \quad H \geq H_r .$$

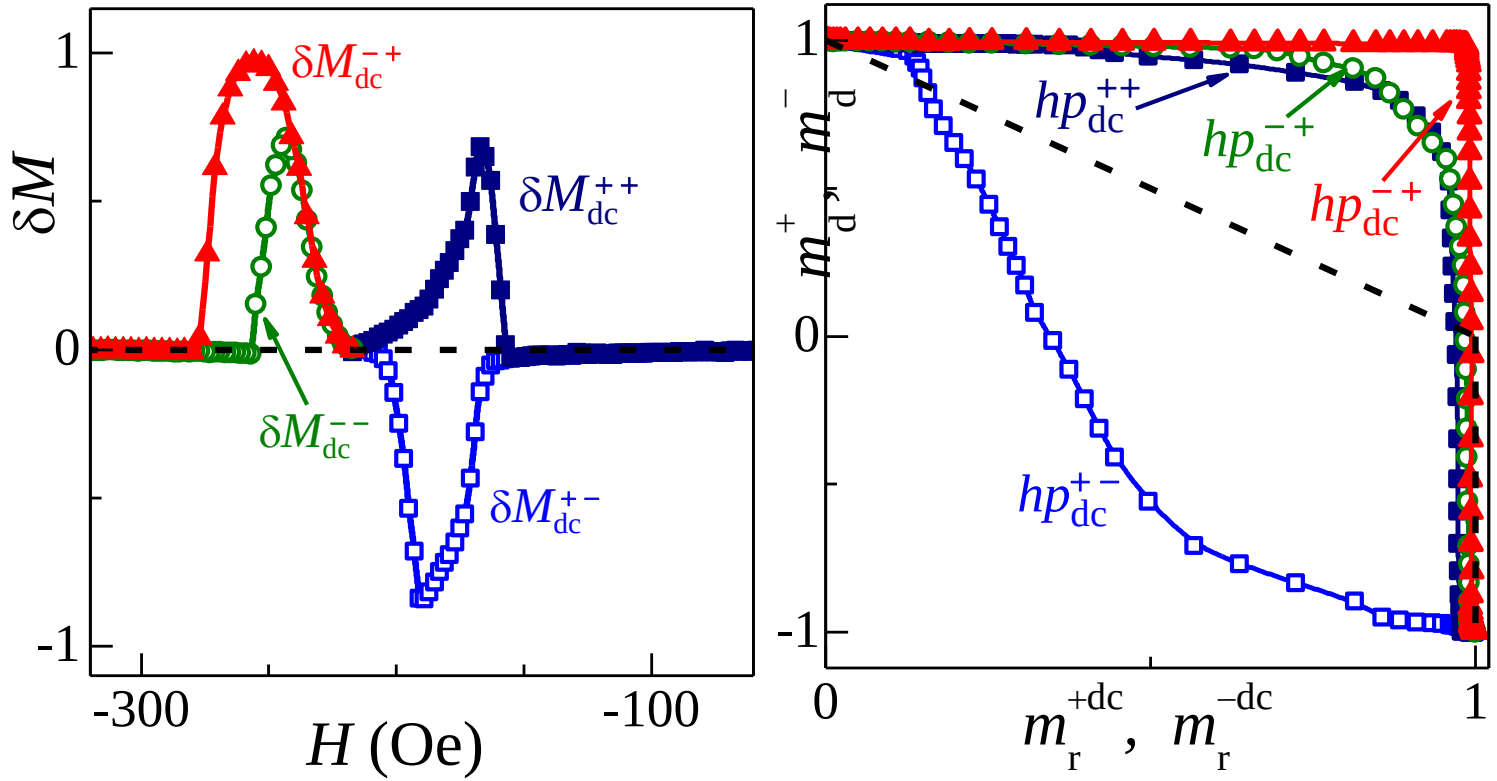

Biased asymmetric loops (EB):

New graphs:

$$\Delta m_r(H) = m_r^-(H) - m_r^+(H)$$

$$\Delta m_d(H) = m_d^-(H) - m_d^+(H)$$

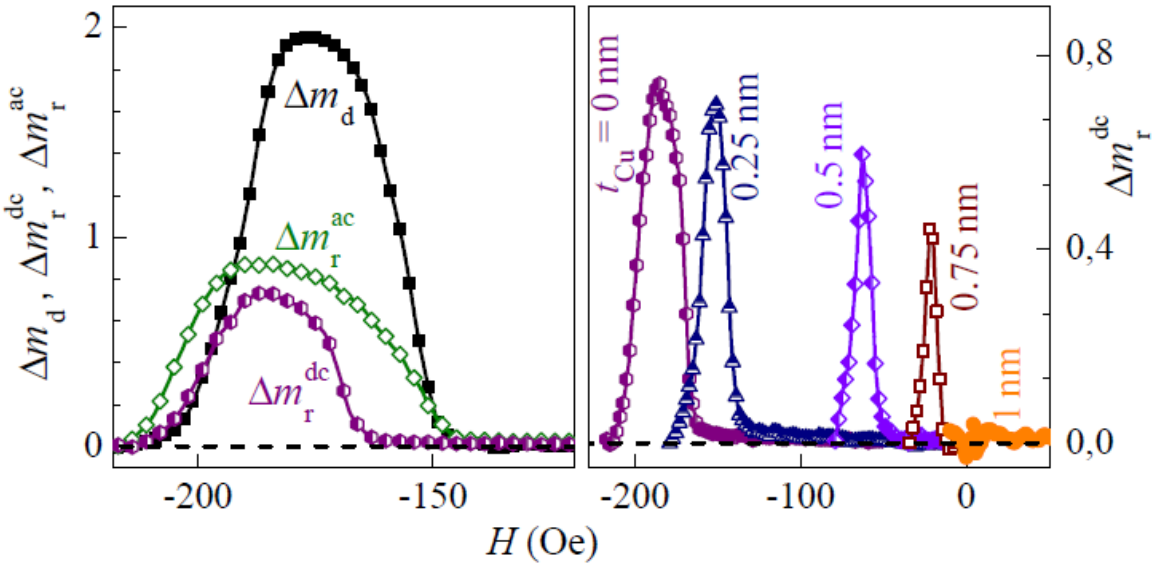

A. Harres, R. Cichelero, L. G. Pereira, J. E. Schmidt, and J. Geshev, "Remanence plots technique extended to exchange bias systems," Journal of Applied Physics **114** (2013) 043902.

Biased asymmetric loops (EB):

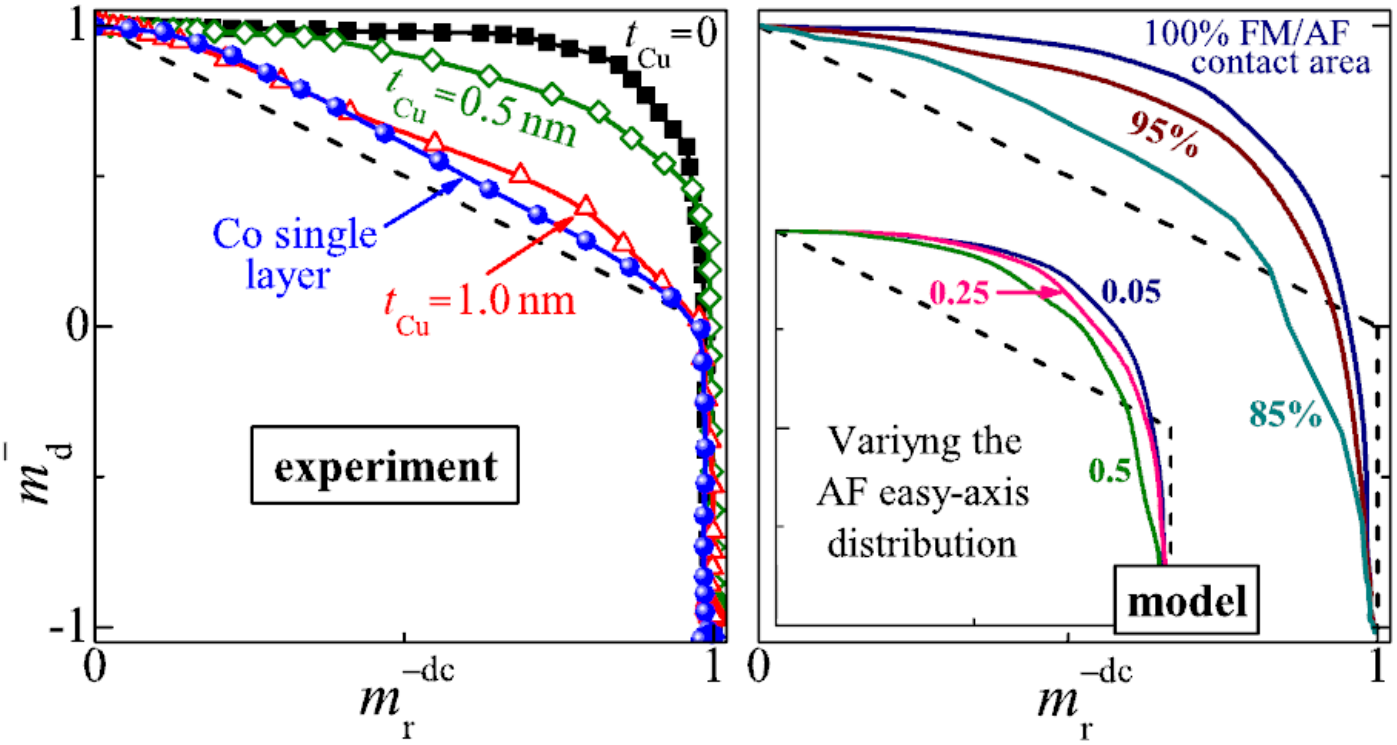

A. Harres, R. Cichelero, L. G. Pereira, J. E. Schmidt, and J. Geshev, "Remanence plots technique extended to exchange bias systems," Journal of Applied Physics **114** (2013) 043902.

Summary: Remanence plots of exchange-coupled systems:

- ✓ The deviations of the experimental from the theoretical plots could give information about the reversal mechanism that dominates at each branch of the hysteresis loops and the interactions present, i.e., exchange and/or dipolar coupling;
- ✓ Outcomes of interactions within the FM could be distinguished from those coming from coupling at the FM/AF interface;
- ✓ Demagnetizing interaction effects could be achieved without the presence of dipolar interactions;
- ✓ Such experiments could give selectively information on modifications caused by a post-deposition treatment in each layer of the film.

Maximizing H_{EB}: light-ion irradiation: thermal aftereffect problem

H_{eb} versus time after irradiation: bottom-pinned FM

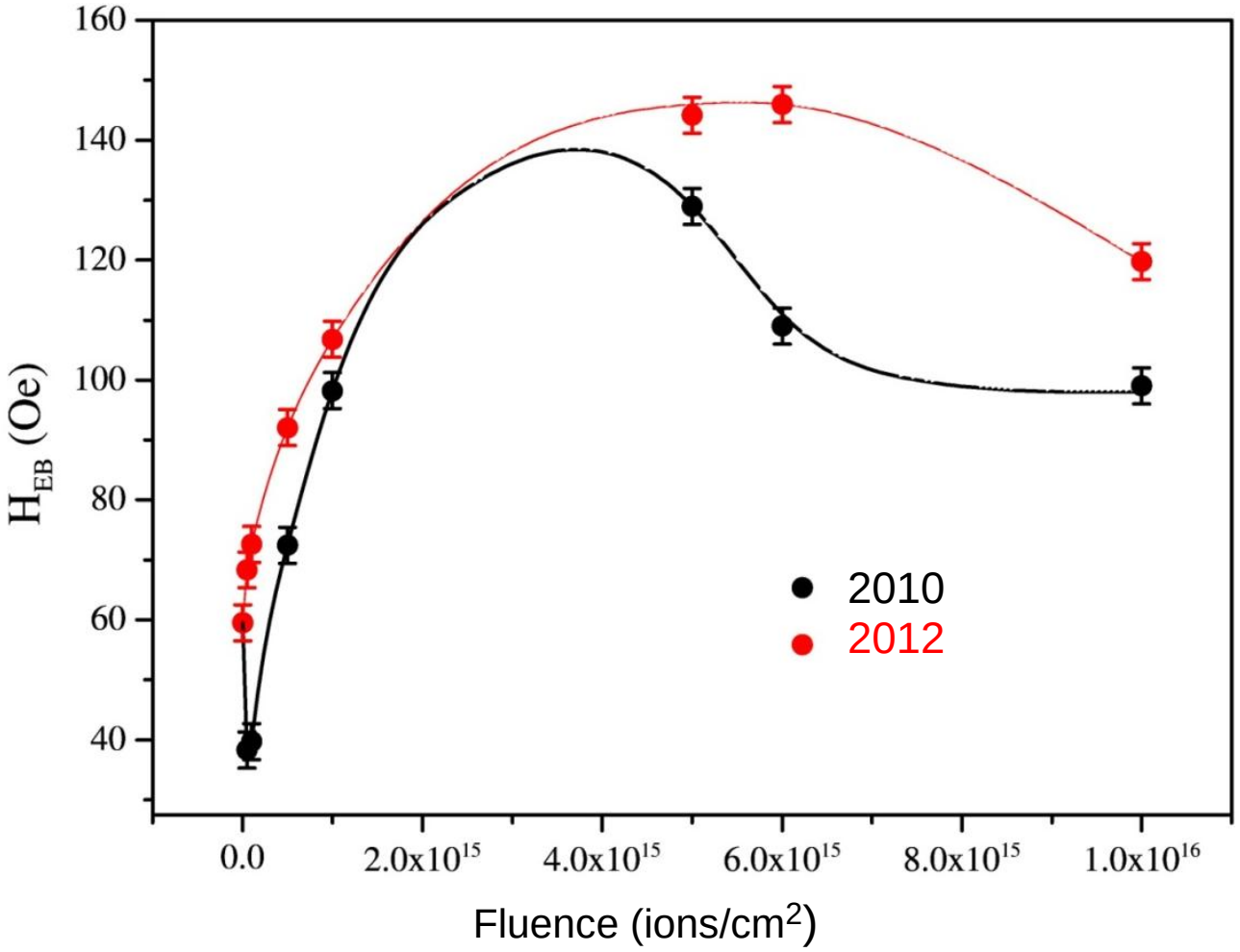

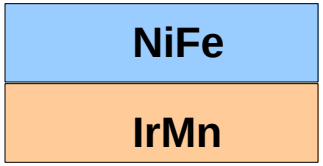

H_{eb} versus time after irradiation: top-pinned FM

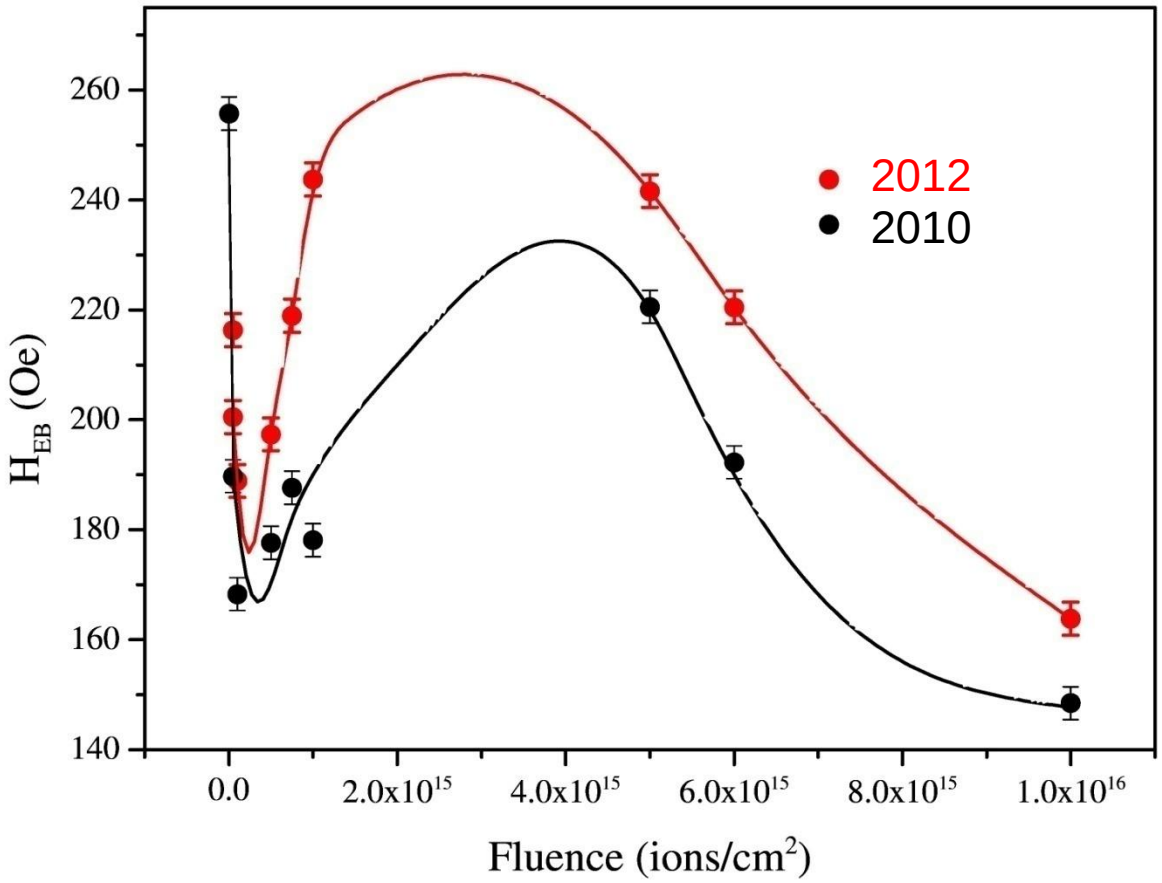

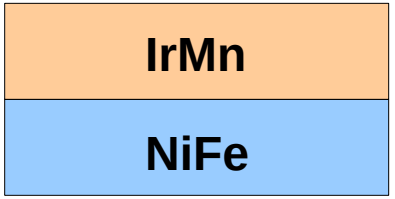

H_{eb} versus time after irradiation: top-pinned FM

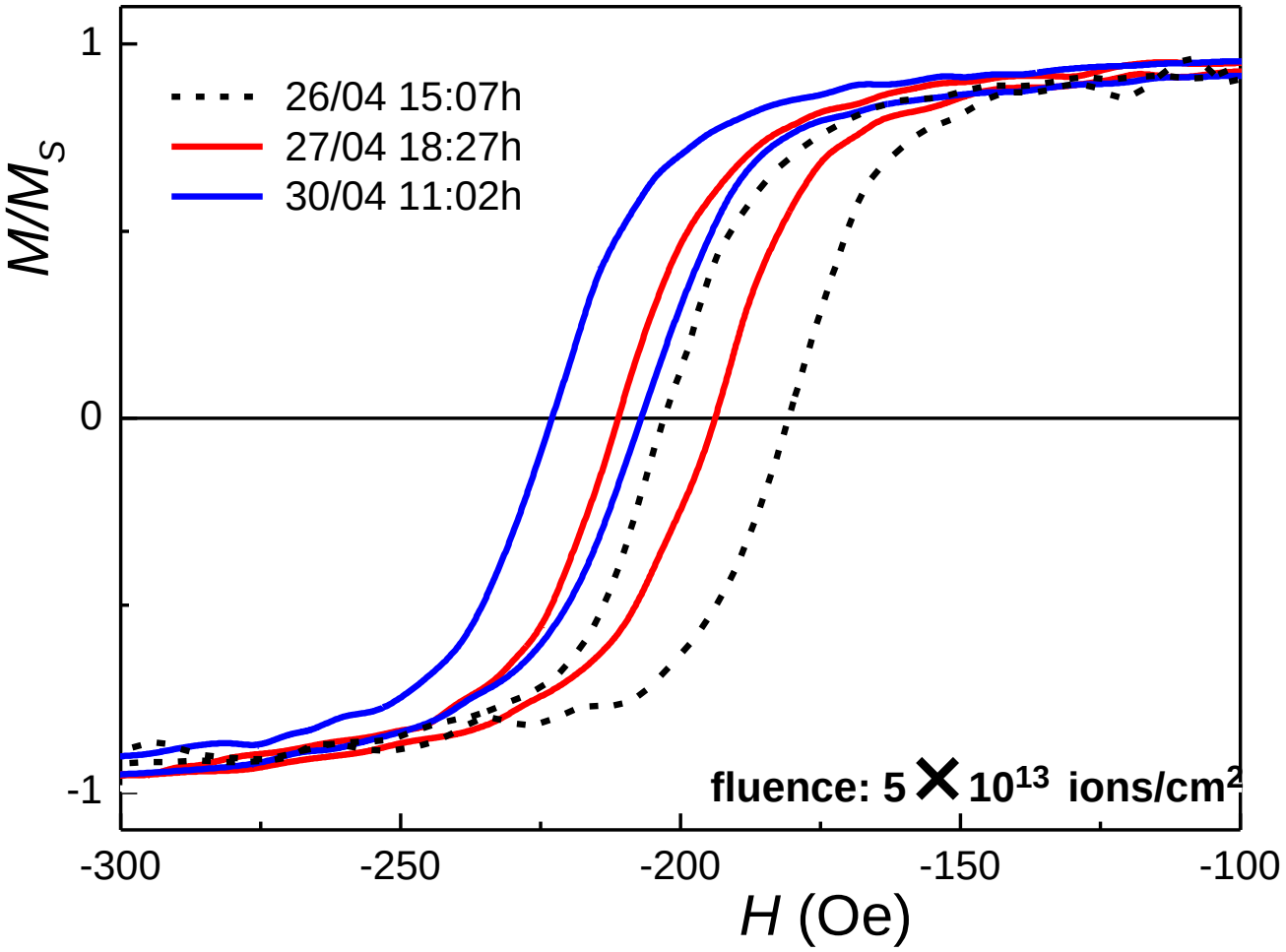

The field-annealed films didn't show such an effect.

Thermal aftereffect:

1961: Jacobs and Kouvel: the thermal aftereffect in the AF in AF/FM systems changes the exchange constant J – ***extraordinary aftereffect***.

I. S. Jacobs and J. S. Kouvel, Phys. Rev. **122**, 412 (1961).

1972: Fulcomer and Charap, based on the Néel's work [L. Néel, Ann. Phys. (Paris) 2, 61 (1967)], developed the Thermal fluctuation aftereffect model (FC model) for FM/AF systems.

E. Fulcomer and S. H. Charap, J. Appl. Phys. **43**, 4190 (1972).

1998: Fujikata et al. used the FC model to explain the annealing time (t_{ann}) dependent change of H_{EB}.

J. Fujikata et al., J. Appl. Phys. **83,** 7210 (1998):

$$H_{EB}/H_{EB}(0) = h + K\ln(t),$$

where K increases with t_{ann}.

2002: Thermally-activated self-alignment processes in NiO/FM, where FM = NiFe, Fe, Ni, or Co

As-made films stored at different temperatures, H_{ann} **parallel** to the initial EB direction.

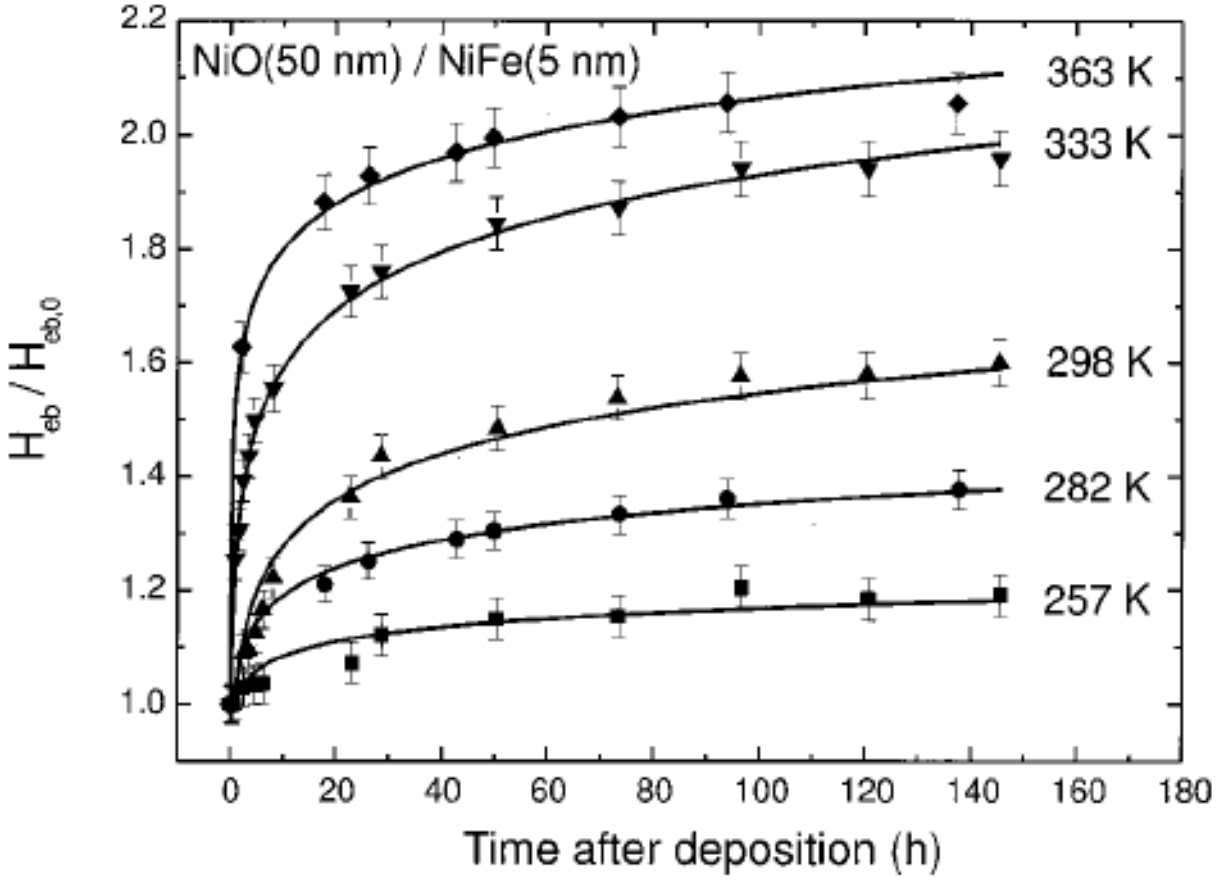

Lines:
ln(*t*) fits through the FC model.

A. Paetzold and K. Röll, J. Appl. Phys. **91** 7748 (2002).

As-made films stored at different temperatures, **H_{ann} antiparallel** to the initial EB direction.

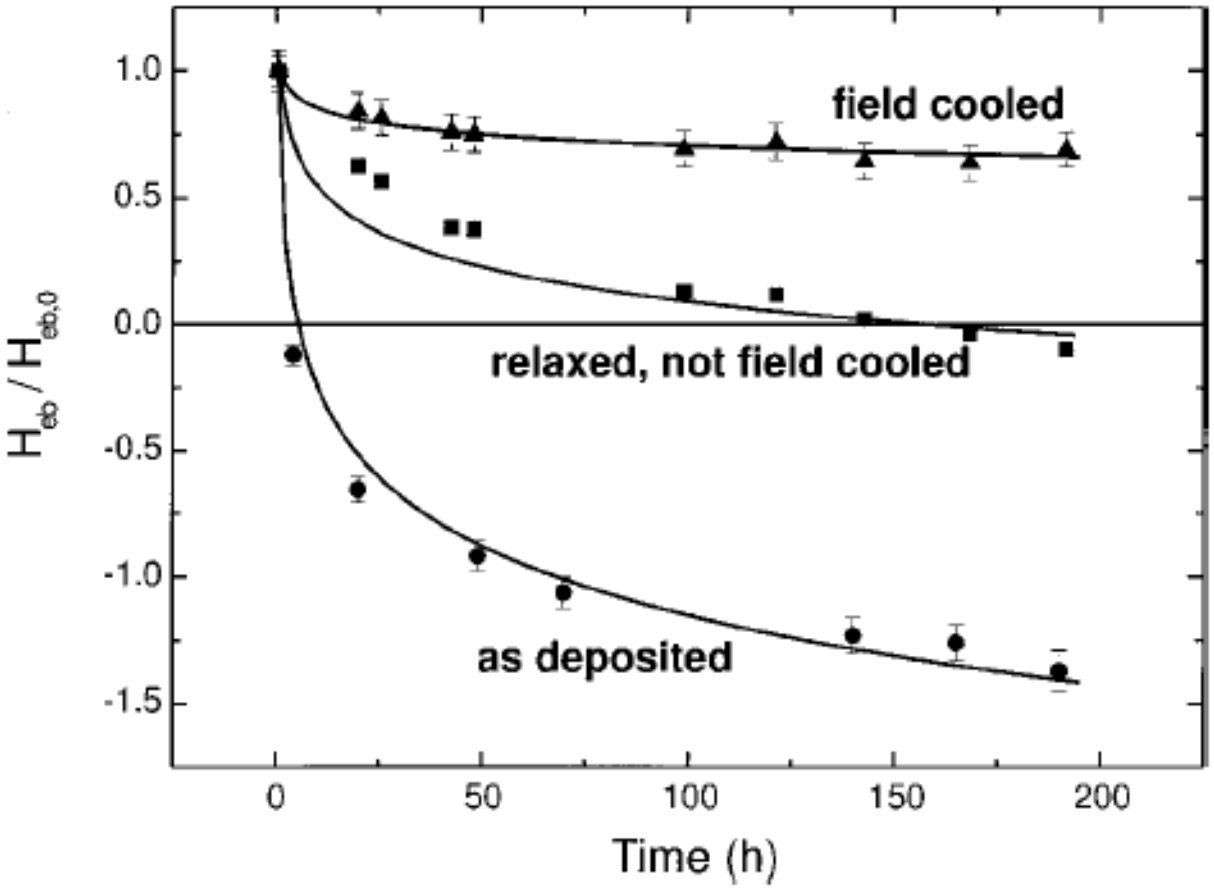

Lines:
ln(*t*) fits through the FC model.

A. Paetzold and K. Röll, J. Appl. Phys. **91** 7748 (2002).

Since 2005: The group of Arno Ehresmann in Kassel, Germany:

Light-ions irradiation of already annealed films.

They used

- different ion bombardment (IB) fluences;
- different storage temperatures;
- parallel or antiparallel $\mathbf{H_{IB}}$ and $\mathbf{H_{EB}}$ configurations.

Ehresmann et al. have proposed a model also based on that of FC: interplay between the ion-bombardment-decreased K_{AF}, modified J, and relaxation time distributions influencing the thermal drift.

J. Appl. Phys. **109**, 0232910 (2011)

$$H_{EB}(t)/H_{EB,0} = h + \Delta h \ln(t),$$

where

$$\Delta h \approx \frac{J\ T}{M_{FM}\ t_{FM}\ K_{AF}}.$$

H_{eb} versus time, different aging temperatures

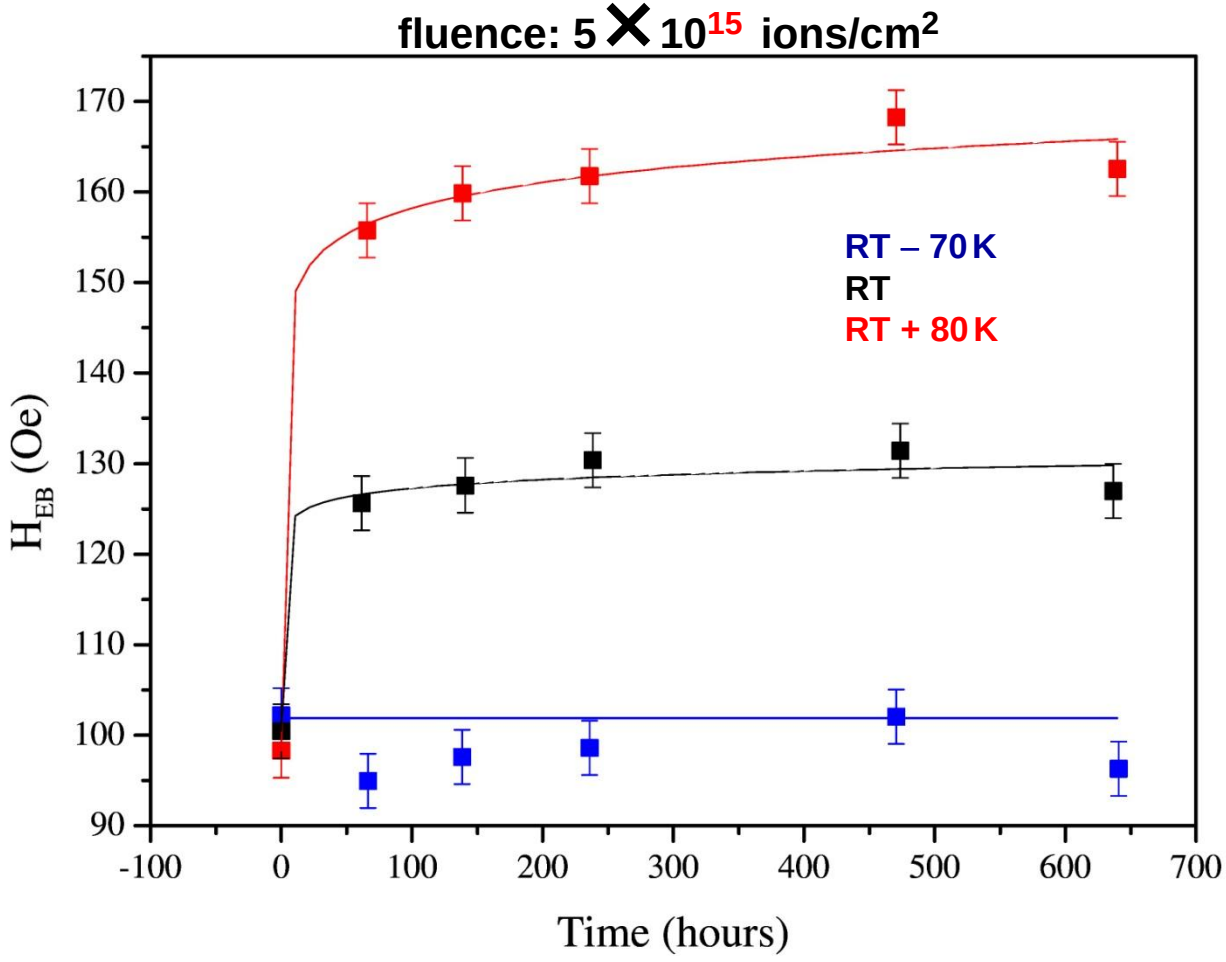

Our samples:
bottom-pinned

NiFe(5 nm)
IrMn (15 nm)

H_{eb} versus time, different aging temperatures

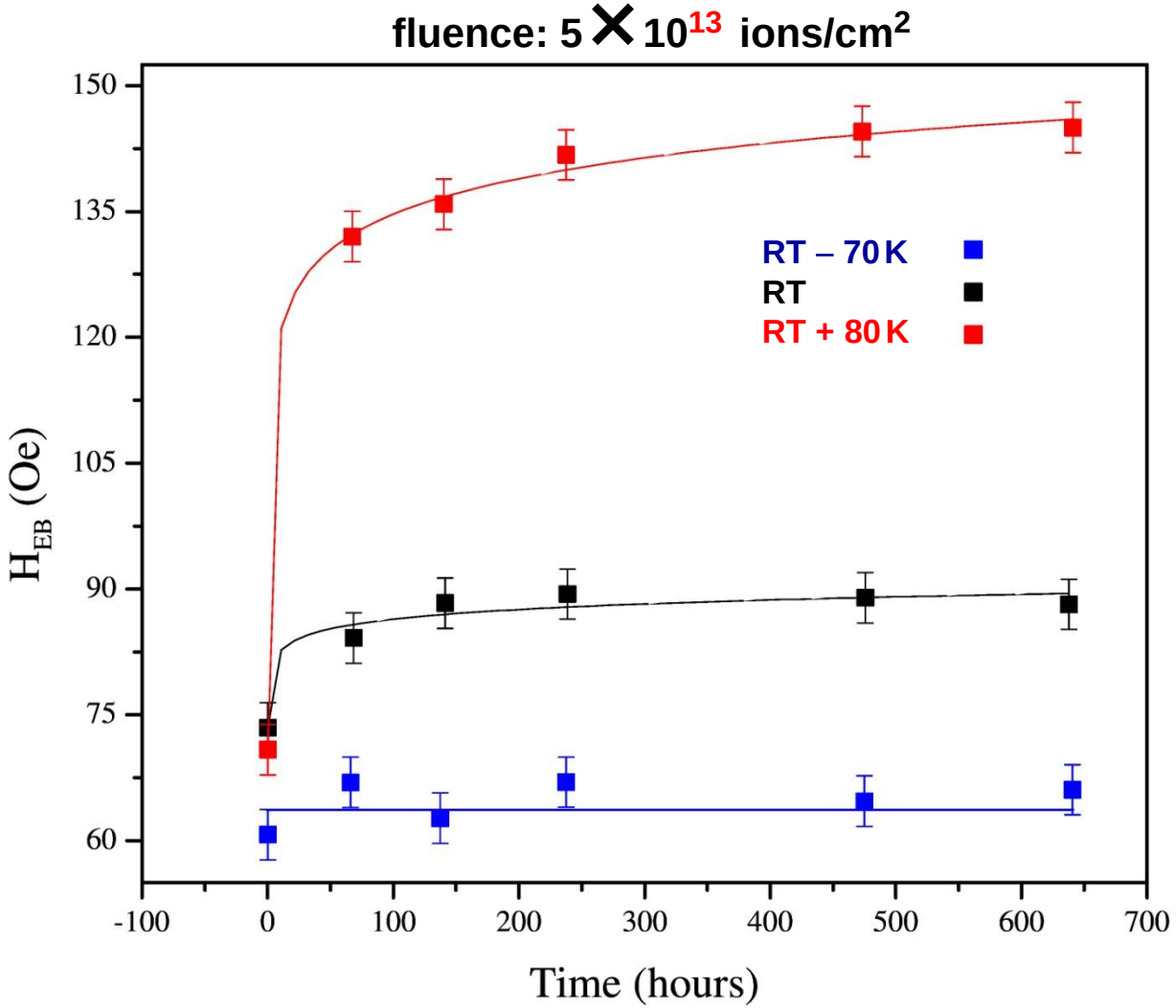

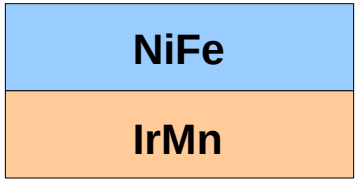

Our films:

- ✓ IrMn/Co and IrMn/Cu/Co
- ✓ NiFe/IrMn and InMn/NiFe

Main results:

- ✓ No ‘classic’ training effect
- ✓ Complete reorientation of the EB direction by IB
- ✓ H_{EB} immediately after IB greater than that achieved after annealing
- ✓ H_{EB} increases significantly with time after IB (more than 2×)
- ✓ The effect of the current during IB is very weak; no effect on Δh
- ✓ Defects created during IB cause the H_{EB} enhancement

Open questions:

- ✓ **What kind of defects are created by IB and where?**
  XRD, MEIS, XANES
- ✓ **Why H_C remains ≈ constant while H_{EB} increases with t?**
  FMR results (H_{res} versus the in-plane angle of H)
- ✓ **Is H_{IB} essential for the EB increase with t after IB?**
- ✓ **Is Δh due to newly-relaxed coupling sites?**
- ✓ **Is H applied during aging important?**

Is H_{IB} essential for the EB increase with *t* after IB?

Our results strongly indicate that
the answer is NO:

In 2008, a piece of an as-made IrMn/Cu/Co film was irradiated with He^+ with no **H** applied. H_{EB} measured in 2012 is 2× bigger.

- ✓ **Is H_{EB} modified due to newly-relaxed spins only?**
  (seems to be true for magnetically saturated FM layers)

- ✓ **Is *H*, applied during aging, important?**

The same experiment on almost relaxed sample (600h of aging):
10% decrease of H_{EB}

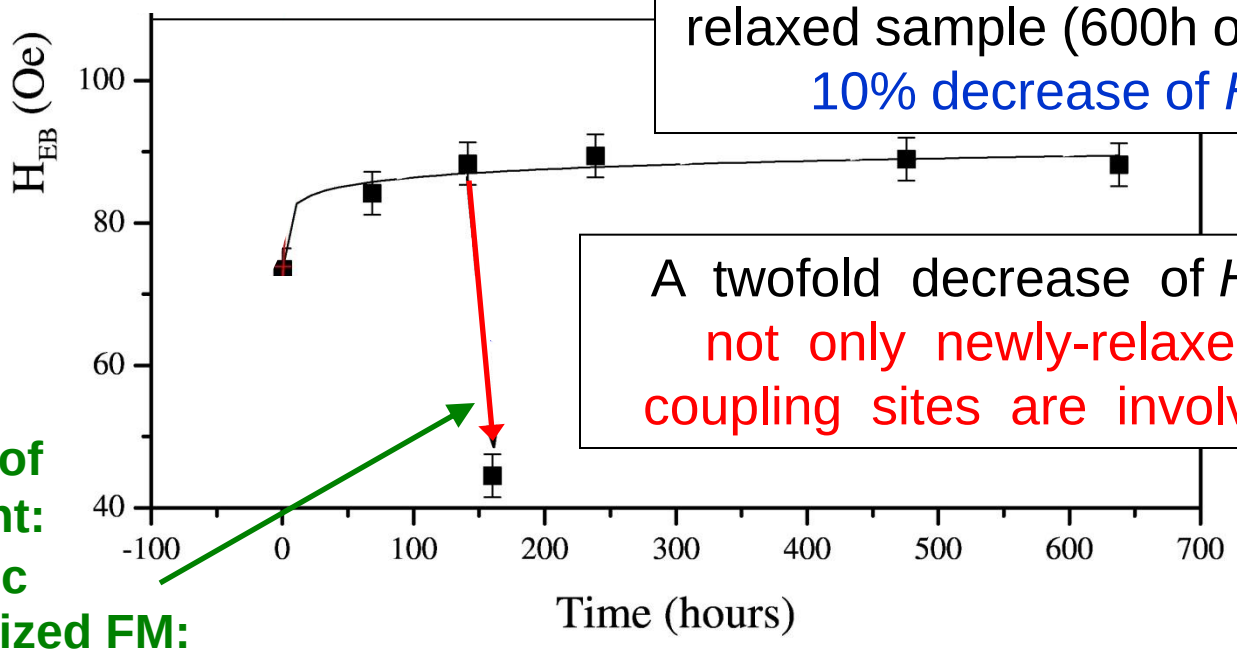

A twofold decrease of H_{EB}:
not only newly-relaxed coupling sites are involved!

New type of experiment:
aging of dc demagnetized FM:

Irradiation-induced EB aging effect: **Summary**

- ✓ H_{EB} immediately after IB is greater than after annealing: *IB is the method to be used – no major structural changes made*
- ✓ H_{EB} increases *significantly* with time after IB (more than 2×) while H_C does not change significantly
- ✓ The effect of the current during IB is very weak; no effect on the H_{EB} rise
- ✓ Defects created during IB cause the H_{EB} enhancement

  (what kind of defects are created and where – to be studied)
- ✓ H_{IB} does not influence the EB increase with t
- ✓ H , applied during aging, is not important:
  what matters is the magnetization state of the FM layer
- ✓ Not only new coupling sites can be involved in the H_{EB} changes

Mais desafios:

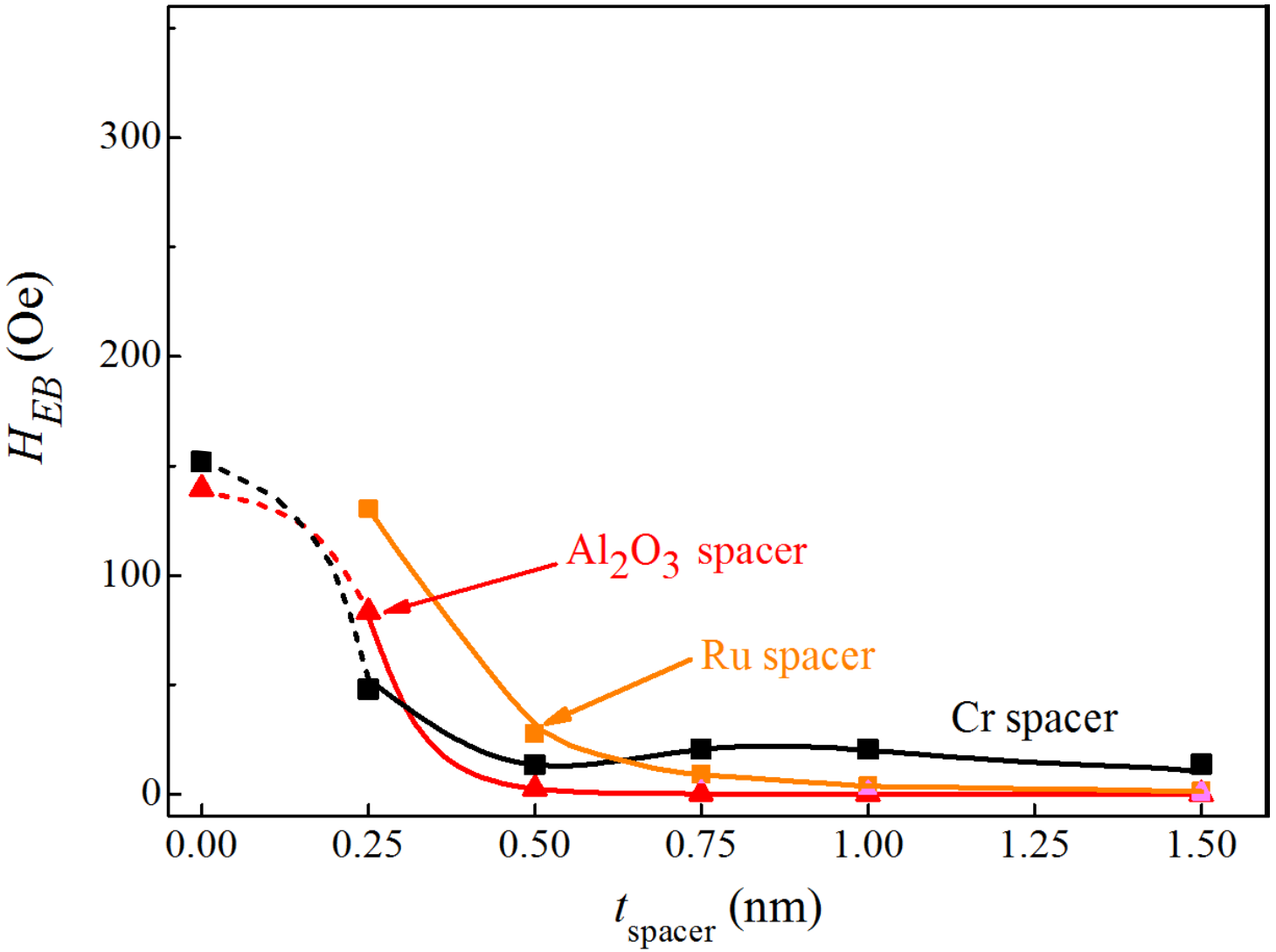

Thanks!